DISSERTATIONES
TECHNOLOGIAE
CIRCUMIECTORUM
UNIVERSITATIS
TARTUENSIS
39

MIRJAM UUSÕUE

Suspended particles dynamics and characteristics in optically complex waterbodies

DISSERTATIONES TECHNOLOGIAE CIRCUMIECTORUM
UNIVERSITATIS TARTUENSIS
39

DISSERTATIONES TECHNOLOGIAE CIRCUMIECTORUM
UNIVERSITATIS TARTUENSIS
39

MIRJAM UUSÕUE

Suspended particles dynamics and characteristics in optically complex waterbodies

UNIVERSITY OF TARTU
Press
1632

Estonian Marine Institute and Department of Zoology, Institute of Ecology and Earth Sciences, Faculty of Science and Technology, University of Tartu, Estonia

Dissertation was accepted for the commencement of the degree of *Doctor philosophiae* in environmental technology at the University of Tartu on 03.04.2023 to 06.04.2023 by the Scientific Council on Environmental Technology, University of Tartu.

Supervisors:	Associate Professor Martin Ligi, University of Tartu, Estonia
	Prof. Tiit Kutser, University of Tartu, Estonia
	Assistant Professor François Bourrin, University of Perpignan, France
Opponent:	Dr. Therese Harvey, Norwegian Institute for Water Research (NIVA), Norway
Commencement:	Room 127, 2 Juhan Liivi Street, Tartu, on 10th May 2023 at 12.15 a.m.

Publication of this thesis is granted by the Institute of Ecology and Earth Sciences, University of Tartu

ISSN 1736-3349 (print)
ISBN 978-9916-27-177-3 (print)
ISSN 2806-2612 (pdf)
ISBN 978-9916-27-178-0 (pdf)

University of Tartu Press
www.tyk.ee

TABLE OF CONTENTS

LIST OF ORIGINAL PUBLICATIONS

This thesis is based on the following publications:

I Bourrin, F., **Uusõue, M**., Artigas, M.C., Sànchez-Vidal, A., Aubert, D., Menniti, C., Klar, J. (2021). Release of particles and metals into seawater following sediment resuspension of a coastal mine tailings disposal off Portmán Bay, Southern Spain. *Environmental Science and Pollution Research* 28, 47973–47990, https://doi.org/10.1007/s11356-021-14006-1

II Uudeberg, K., Aavaste, A., Kõks, K.-L., Ansper, A., **Uusõue, M**., Kangro, K., Ansko, I., Ligi, M., Toming, K., Reinart, A. (2020). Optical water type guided approach to estimate optical water quality parameters. *Remote Sensing* 12, 931, https://doi.org/10.3390/rs12060931

III **Uusõue, M**., Ligi, M., Kutser, T., Bourrin, F., Uudeberg, K., Kangro, K., Paavel, B. (2022). Effects of different conditions on particle dynamics and properties in West-Estonian coastal areas. *Oceanologia*. https://doi.org/10.1016/j.oceano.2022.06.006

Author's contribution

This thesis is based on the publications that are the result of a collaborative effort in which all authors participated.

I The idea for this study came from F. Bourrin. He was also the principal author of the paper. M. Uusõue had a significant role in data processing and analysis of experiments T1 and T2 (current profiles, characterisation of sediment plumes and particles, laboratory analyses of disaggregated grain size spectra) and had a minor part in writing, editing, and reviewing the manuscript.

II The idea for this study came from K. Uudeberg. M. Uusõue participated in obtaining information (including fieldwork) and extracting Sentinel-3 satellite data. She had a minor part in writing, editing, and reviewing the manuscript.

III The idea for this study came from M. Uusõue. She was responsible for the planning and design of the study. She participated in the fieldwork, prepared and analysed the data, and wrote the original draft of the article. M. Ligi, T. Kutser, and F. Bourrin supervised the work.

ABBREVIATIONS AND ACRONYMS

$a(\lambda)$	spectral absorption coefficient (m^{-1})
$a_p(\lambda)$	spectral particulate absorption coefficient (m^{-1})
$b(\lambda)$	spectral scattering coefficient (m^{-1})
$b_b(\lambda)$	spectral backscattering coefficient (m^{-1})
$b_p(\lambda)$	spectral particulate scattering coefficient (m^{-1})
$b_p^*(\lambda)$	mass-specific spectral particulate scattering coefficient ($m^{-2} \cdot g^{-1}$)
$b_{bp}(\lambda)$	spectral particulate backscattering coefficient (m^{-1})
$b_{bp}^*(\lambda)$	mass-specific spectral particulate backscattering coefficient ($m^{-2} \cdot g^{-1}$)
$b_{bp}/b_p(\lambda)$	spectral particulate backscattering ratio
λ	wavelength (nm)
$c(\lambda)$	spectral attenuation coefficient (m^{-1})
C2RCC	Case2Regional CoastColour
CDOM	coloured dissolved organic matter
Chl-a	chlorophyll-a
D50	median particle size distribution
DIGS	disaggregated grain size spectra
$Ed(0+, \lambda)$	spectral downwelling irradiance
ENVISAT	Environmental Satellite
ESA	European Space Agency
IOPs	inherent optical properties
j	Junge exponent
Lu	Spectral upwelling radiance
MERIS	Medium Resolution Imaging Spectrometer
OAS	optically active substances
OLCI	Ocean and Land Colour Imager
OWT	optical water type
PSD	particle size distribution
$R(\lambda)$	spectral water-leaving reflectance
Rrs	remote sensing reflectance
SPIM	suspended particulate inorganic matter ($mg \cdot L^{-1}$)
SPM	suspended particulate matter ($mg \cdot L^{-1}$)
SPOM	suspended particulate organic matter ($mg \cdot L^{-1}$)
TSM	total suspended matter ($mg \cdot L^{-1}$)

1. INTRODUCTION

Coastal areas are socio-economically important for urban development, tourism, transport, marine construction and renewable energy. Often, water quality in these areas deteriorates due to intensive use, which directly affects their ecosystem (Biswas & Tortajada, 2019; Fan et al., 2022; Hettige et al., 2014). Water degradation is also linked to agricultural activities, such as using large amounts of fertilisers, which lead to higher levels of nutrients in the water, resulting in algal blooms (Bordenave et al., 2020; Mateo-Sagasta et al., 2017; Zia et al., 2013). Water transparency is linked to water quality and decreases during algal and cyanobacterial blooms and when the concentration of coloured dissolved organic matter or resuspended particles in water increases (Capuzzo et al., 2015; Davies-Colley & Smith, 2002; Kahru et al., 2022). Poor farming practices lead to the erosion of terrigenous material containing chemical and biological contaminants, which is transported to coastal areas by rivers and surface runoff (Mateo-Sagasta et al., 2017). Dredging and trawling lead to the resuspension of bottom sediments (Chen et al., 2020; Durrieu De Madron et al., 2005; Hayes et al., 2000; Martín et al., 2014; Mengual et al., 2016). Due to climate change, natural events, such as storms and floods, have increased (Hirabayashi et al., 2021; Tabari, 2020). Because of these events, large amounts of debris and particles are transported to coastal areas by rivers or resuspended from the seabed.

The particles resuspended by the above-mentioned human activities or natural events are considered harmful to the environment because they can transport sorbed trace metals (Tessier, 1992) and other toxic organic substances. Trace metals are transported by sediments near mining sites located in coastal areas or on the seabed. Mined ores in the deep sea and old mining sites which could be exploited again are, for example, massive sulphides, ferromanganese nodules and a cobalt-rich crust formed over geological time periods (McMurtry, 2019; Miller et al., 2018; Van Dover, 2011). Mining activities in the deep sea are large-scale, intensive and destructive, and their environmental impacts are poorly understood and difficult to study (Hannington et al., 2011; Hein et al., 2013). In addition, sediments deposited on seabed vegetation can damage the entire aquatic ecosystem, and increased turbidity caused by high concentrations of suspended sediments prevents predatory fish from feeding (Erftemeijer et al., 2012; Erftemeijer & Robin Lewis, 2006; Hecht & van der Lingen, 1992; Rowe & Dean, 1998).

It is crucial to continuously monitor water quality to better assess the impact of humans and natural events on water bodies and to find appropriate solutions to improve water quality. In situ measurements allow the collecting of precise and detailed information on various water parameters. However, field campaigns are time-consuming and expensive and can only be carried out on a spatially limited scale. Weather is also a limiting factor when conducting field campaigns. Coastal areas are highly dynamic, and the possibility of monitoring temporal changes in processes with in situ measurements is limited. On the other hand, remote sensing can cover large areas with high temporal frequency but with lower

accuracy, and the number of parameters that can be measured is limited. Only visible light can penetrate water and give us information about the water constituents. This, however, means that remote sensing data cannot be collected during the night and through clouds. In summary, remote sensing is a valuable and complementary tool to in situ measurements for monitoring highly dynamic coastal areas.

The European Union's Copernicus Earth observation programme is a new step in using space sensors in Earth observation. It provides long-term funding and continuity of space assets and will allow monitoring of many parameters over several decades (Copernicus, n.d.). Previous ESA and other space agencies' satellites were one-off scientific missions that ended with the lifetime of the respective satellite. The launch of ESA scientific missions will continue, but the aim of Sentinels, launched in the frame of the Copernicus program, is to guarantee continuous availability of selected types of data. Sentinel-3 satellite, launched in 2016, was primarily designed for remote sensing of waters. It has the Ocean and Land Colour Imager (OLCI) on board (ESA, n.d.-b). OLCI, the remote sensing data source for this work, is an improved version of the Medium Resolution Imaging Spectrometer (MERIS) launched on board ENVISAT in 2002 and ended in 2012 (ESA, n.d.-a). There are two identical Sentinel-3 satellites (A and B) in orbit to ensure higher revisit time and data availability in the case where one of the two fails. OLCI has 21 spectral bands with a spatial resolution of 300 m. The constellation revisit time is once per day at the equator and twice per day at our latitudes.

The scheme of the formation of remote sensing signal from the water is represented in the Figure 1. The satellite sensors measure the top of atmosphere radiance, i.e. the amount of solar radiation reflected from the Earth's surface and modified by the atmosphere on the way to the Earth and back to satellite altitude (EOSDIS, n.d.). More than 90% of the radiance measured by satellites above water bodies originates from the atmosphere and contains no information about water properties (Mobley, 2022a). This signal must be removed, and the process is called atmospheric correction. The illumination conditions and atmospheric properties in natural environment vary over time. To make the images comparable for further analysis, one has to remove these variations. Remote sensing reflectance (the ratio between the water-leaving radiance and downwelling solar irradiance) is derived in the process of atmospheric correction.

After the remote sensing signal is calculated, it needs to be analysed and converted into different remote sensing products (Chl-a, SPM, CDOM, turbidity, etc.). This can be done with empirical, analytical, or semi-empirical models, or with different artificial intelligence methods that are briefly summarized in Yang et al. (2022). Simple empirical models use statistical correlation directly between a water parameter of interest and remote sensing signal (the full reflectance spectrum, band-ratios or their combinations) (Matthews, 2011). These models are easy to use, but they are not universal as the relationships between the optical properties and water parameters vary from waterbody to waterbody, and in many waterbodies, may vary also seasonally. Analytical methods use bio-optical or

radiative transfer models and use the full measured spectrum to retrieve water constituents. The use of these analytical methods is limited as they require high-quality reflectance data, which is hard to achieve in optically complex inland and coastal waters as there are no good atmospheric correction methods available for these waters. Analytical methods are computationally expensive, which may cause some problems in the case of large images. Semi-empirical models use a combination of empirical and analytical models. (Hunter et al., 2010). Artificial intelligence models such as Artificial Neural Networks and Support Vector Machines allow to get linear and nonlinear relationships between reflectance and water constituents and, thus, better accuracy. Unfortunately, they need a large amount of in situ data for training, which is hard to get (Mas & Flores, 2008).

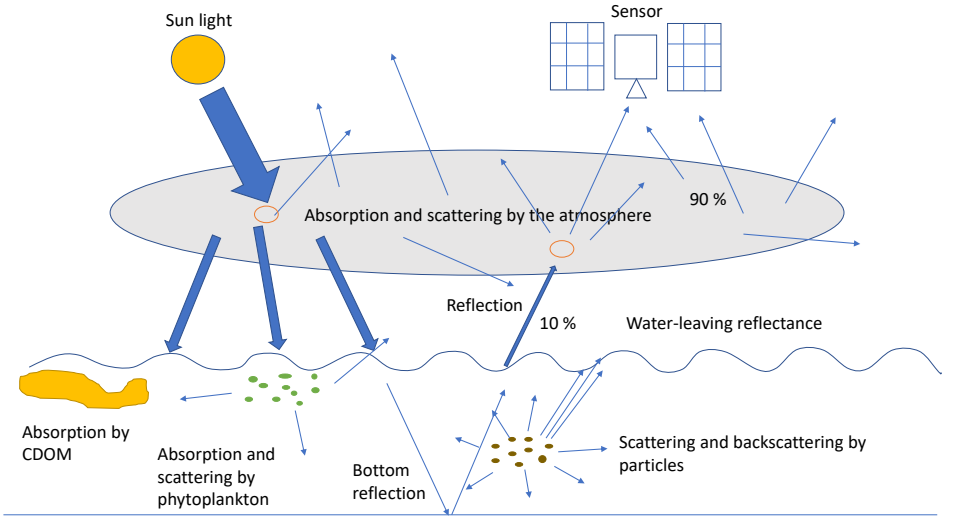

***Figure 1**: Scheme showing the light transfer through different mediums and the impact of these mediums on the light*

Remote sensing reflectance is influenced by water's inherent optical properties (IOPs), such as absorption, scattering, and backscattering (Mobley, 1994). The optical properties of the water depend on the optically active substances (OAS) that interact with the light. One classification approach divides OAS into three types: phytoplankton, suspended particulate matter (SPM), and dissolved coloured organic matter (CDOM) (Prieur, 1981). Phytoplankton are unicellular algae, and one of their photosynthetic pigments, chlorophyll-a (Chl-a), is used as one of the proxies to determine phytoplankton biomass (Duckey et al., 2006). Chl-a absorbs light in the blue (around 420–430 nm) and red regions (around 670 nm) of the visible light spectrum (Kirk, 2011). SPM consists of suspended particulate inorganic matter (SPIM), such as mineral particles, and suspended particulate organic matter (SPOM), such as phytoplankton cells, non-living cellular matter, zooplankton, and organic detritus (Mobley, 1994, 2022b). SPM mainly scatters light but also absorbs it. SPOM absorbs light at all wavelengths and has similar

absorption spectra to CDOM (maximum in the ultraviolet (UV) and exponentially decreasing with increasing wavelength). Some mineral fractions of the SPM not only scatter light strongly but absorb it. For example, red clay has high absorption values in the UV and blue regions of the light spectrum, and absorption decreases at longer wavelengths (Kako et al., 2019). CDOM is the product of decaying material (phytoplankton, zooplankton, plants, soils) and absorbs light (Coble, 2007). Light absorption by CDOM is most significant in the UV and blue regions of the light spectrum and decreases exponentially towards longer wavelengths (Mobley, 1994, 2022b). In the open ocean, organic detritus and CDOM produced by zooplankton grazing or algal cell decay are derivative products of phytoplankton. Therefore Chl-a can be used as a proxy to estimate these products (Kirk, 2011). In coastal areas, phytoplankton, SPM and CDOM contribute independently to optical properties. It is hard to separate the contribution of each OAS from their cumulative impact on water colour (reflectance spectrum) as many different combinations of OAS may result in an identical reflectance. Therefore, such waters are considered optically complex (Morel & Prieur, 1977). Consequently, it is essential to study the properties of each substance in detail and find out how they affect the remote sensing signal, as this will enable more accurate retrieval of OAS from the remote sensing signal.

In this study, the main focus is on the properties of SPM. SPM affects the remote sensing signal in complex ways. Its ability to scatter light depends on its properties, such as shape, size distribution, type and concentration. Smaller particles, < 10 μm, scatter strongly at shorter wavelengths. The scattering capacity of coarser particles cannot be directly related to wavelength (Pozdnyakov & Graßl, 2003). Organic particles absorb more light than they scatter, while mineral particles mainly scatter light (Kirk, 2011). In addition, under certain conditions (high salinity gradient, high concentrations of organic matter and high particle concentrations), the primary particles tend to aggregate into flocs that can break apart when mechanically disturbed (Mobley, 1994, 2022b). This process leads to significant variations in the water constituents' optical properties and complicates the scattering properties' study. Although complicated, the variability of IOPs associated with particles has been studied around the world and also in the optically complex Baltic Sea (Berthon & Zibordi, 2010; Freda, 2012; Kratzer & Moore, 2018; Kutser et al., 2009; Lee et al., 2019; Many et al., 2016; Paavel et al., 2011; Wolanskit & Gibbst, 1995; Woźniak et al., 2011; Woźniak et al., 2018, 2022).

One of the properties that has long been under investigation is the particulate backscattering ratio (particulate backscattering divided by particulate scattering) (e.g. Boss et al., 2004; Loisel et al., 2007; Sun et al., 2019; Ulloa et al., 1994). It is often used in bio-optical models and remote sensing algorithms as a constant that allows SPM concentrations to be derived (J. T. . Kirk, 1981; Stramska et al., 2000; Whitmire et al., 2007). In reality, the ratio depends on the particles' size distribution, shape, and refractive index (Chami et al., 2005; Mckee & Cunningham, 2005). Conversely, it gives an indication of the particle size distribution and the origin of the particles (Aas et al., 2005; Boss et al., 2004).

Deriving accurate remote sensing products such as SPM concentrations is complicated in optically complex waters, besides the above-described reasons, also due to problems with the complexity of SPM properties. Standard remote sensing algorithms often fail in coastal and inland waters (Ligi et al., 2017; Ohde et al., 2007; Soomets et al., 2022; Toming et al., 2017). Also, local algorithms have been developed, but they do not always allow us to obtain correct results, especially in rapidly changing conditions. For example, the best correlations with in situ SPM concentrations observed by Ligi et al. (2017) were obtained with Dekker et al. (2002) model (R^2 = 0.29). Toming et al. (2017) tested band ratios of R709/R754 and R665/R560 on OLCI images processed with C2RCC atmospheric correction processor. They got better results with R^2=0.49 and R^2=0.69, respectively, when the in situ data from different sources was merged. The problem with SPM algorithms is that SPM in the Baltic Sea coastal areas is composed of organic and mineral particles in variable fractions, and these particles impact remote sensing signal differently.

The problems in deriving accurate water parameters from remote sensing led to several options being considered. An optical water type (OWT)-guided approach was tested in this study. It consisted of reflectance-based optical water type classification applicable to optically complex waters in the boreal region (Uudeberg et al., 2019). Water type-specific empirical SPM models were applied to these OWTs. The hypothesis is that the OWT-guided approach performs better than a single algorithm approach and provides accurate indications of the dynamics of the remote sensing products (SPM in this study). Thus, the main problems, such as how SPM properties (concentration, optical properties, particle size distributions) variability influence remote sensing signal, still need to be solved. Further detailed investigation of the OAS needs to be done. Therefore, additional data on particle size distributions (PSDs) and IOPs associated with the particles were collected from optically different waters to investigate their variability under different conditions further. For the first time, PSDs were measured in the Pärnu Bay, an Estonian coastal area. A disaggregation study was also conducted for the first time. The hypothesis that the backscattering ratio is not a constant and varies significantly in optically complex coastal areas under different conditions was also tested.

Finally, particle properties (PSD and composition) and their environmental impact were studied. For this purpose, a bottom trawling experiment was conducted in the Portman Bay, Spain, polluted by mining for several decades, to investigate the behaviour of suspended polluted sediments in the water column after they have been mechanically stirred up from the seabed.

2. OBJECTIVES

The main objective of this work was to investigate the variability of suspended particulate matter dynamics and optical properties in optically complex waters to understand better their effects on remote sensing signal and the environment.
The objectives of this study were:

- investigate the variability of optical properties of suspended particles under different conditions in optically complex waters of the Baltic Sea coast (**III**)
- characterise the particulate backscattering ratio in dynamic, optically complex coastal areas in order to improve remote sensing methods (**III**)
- testing whether the optical water types guided approach can provide better suspended matter retrievals from satellite imagery than empirical approaches **(II)**
- study suspended particles' spatial distribution in the highly dynamic, optically complex coastal area (**II**)
- investigate the influence of natural disturbance events on the size distribution of resuspended particles in a coastal area with brackish water (**III**)
- investigate the properties, behaviour and impact on the aquatic environment of the particles resuspended by mechanical disturbance activity in a highly contaminated coastal area (**I**)

3. MATERIALS AND METHODS

3.1. Study areas

The study areas of this work are located in the Baltic Sea (Pärnu, Matsalu, and Haapsalu Bays in Estonia – Papers **II** and **III**) and the Mediterranean Sea (Portmán Bay in southern Spain – Paper **I**).

The Baltic Sea is a unique sea with brackish water and a high inflow of rivers compared to its surface area. The rivers transport large amounts of CDOM into the Baltic Sea (Kowalczuk, 1999). Two types of blooms occur in the Baltic Sea. Spring blooms occur between March and June, depending on the location and contain mainly diatoms and dinoflagellates (Klais et al., 2011). In summer, extensive cyanobacterial blooms occur due to the high amount of nutrients (Bianchi et al., 2000; Matti Kahru et al., 1994). Therefore, the Baltic Sea is considered an optically complex water body.

Pärnu, Matsalu, and Haapsalu bays are located on the west coast of Estonia (Figure 2 A-C). The average depth of the Pärnu Bay is 4.7 m (maximum 8 m). The bottom sediments of the Pärnu Bay consist of clay, mud and fine sand. Due to the shallow water depth and openness to the frequent westerly winds, wind-induced resuspension of particles occurs daily. Pärnu Bay is also influenced by the inflow of the Pärnu River (144 km long; mean discharge of 64 m^3/s; the catchment area of 6920 m^2, one of the largest in Estonia), which carries CDOM and particles into the bay (Paavel et al., 2011). The water colour of the Pärnu Bay is consequently yellowish-brown. The inflow of the river also affects the salinity, which is lower (3.5 psu) than outside the bay in the Gulf of Riga (4.5–6 psu) (Kotta et al., 2008). Pärnu River mouth is located in the city of Pärnu (> 40 000 inhabitants). Tourism develops mainly in summer when over 300 000 people visit the area. Thus, urbanisation and human activities affect the water quality in the bay. Haapsalu Bay is semi-enclosed and very shallow, with an average depth of 3 m (Kotta et al., 2008). The influence of the inflow of the Taebla River is moderate. Due to the segmentation of the bay, salinity varies from ~3 psu in the central and eastern parts to ~7 psu in the open part. Haapsalu Bay is also strongly influenced by human activities. The bays' water quality was ranked as the worst in Estonia in 2015 (EEA, 2015) due to pollution originating from the town of Haapsalu and the discharge of nutrient-rich sediments by the streams. Matsalu Bay, unlike the Pärnu and Haapsalu Bays, is a protected area with limited human activities. It is a very shallow bay with an average depth of 1.5 m (maximum 3 m). The Kasari River aliments the Matsalu Bay with a large amount of CDOM (CDOM absorption values of more than 30 m^{-1} at 420 nm were measured by Kutser et al. (2009)), so the colour of the water is predominantly brown. Salinity is ~0.5 psu near the river mouth but can exceed 6 psu in the western part. The bottom sediments of the Haapsalu and Matsalu bays consist of sands, gravels, and clays.

Pärnu, Haapsalu and Matsalu bays are shallow and wind-driven resuspension affects their transparency daily, especially in the Pärnu Bay. They are also affected by the flux of SPM and CDOM from the rivers. Therefore, these bays are suitable sites to study in detail the properties, dynamics and origin of particles under changing conditions at these sites.

In contrast to the Baltic Sea, the Mediterranean Sea has a very high salinity (38 psu on average), as evaporation significantly exceeds precipitation and river runoff (Barale, 2008). On average, phytoplankton biomass concentration and primary productivity are low due to nutrient deficiencies.

Portmán Bay is located in the province of Murcia in south-eastern Spain, south of Cartagena – La Union Mining District, in the western Mediterranean Sea (Figure 2D).

***Figure 2**: The location of the study areas: A – Haapsalu Bay (ALI on-board of EO-1, 14.07.2002), B – Matsalu Bay (ALI on-board of EO-1, 14.07.2002), C – Pärnu Bay (MSI on-board of Sentinel-2, 29.08.2016), D – Portmán Bay (MSI on-board of Sentinel-2, 04.07.2021)*

The superficial bottom sediment is mainly sand and fine clay (*Masas de Agua Costeras*, n.d.). As there are no river inputs, the salinity is above 37.5 psu. This area is crossed by a 25 km long Sierra de Cartagena mountain range (Conesa et al., 2008). Intensive mining activity in the region ended in 1991. During more than 30 years, about 57 million tonnes of mining waste from the Lavadero refinery were dumped into the bay. The waste filled the bay, and the coastline advanced about 700 m towards the sea (Gómez-García et al., 2015; Manteca et al., 2014). The main components of the waste are associated with silica, phyllosilicates and carbonates and are rich in heavy metals such as Pb, Zn, As, and Cd (Peña et al., 2013). Portmán Bay is the most polluted area in the Mediterranean due to the above-mentioned activities (Martinez-Frias, 1997). Portmán Bay is easily accessible and protected from waves and currents. Therefore, it is a good site to study the behaviour of the contaminated sediments during a disturbance event and the impact of the disturbance on the environment.

3.2. Data

The data were collected to study the properties and dynamics of suspended particles in optically complex coastal areas. However, different approaches were used in the Estonian bays (Papers **II** and **III**) and in the Portmán Bay (Paper **I**). The inherent optical properties and the dynamics of SPM concentration were studied in the Estonian coastal areas. Vertical profiles of the inherent optical properties, such as absorption (a) and attenuation coefficients (c), were measured using WET Labs AC-S (**III**). The scattering coefficients (b) were derived from a and c. The backscattering coefficients (b_b) were measured using WET Labs ECO-BB3 and ECO-VSF3 (**III**). These three instruments were mounted in a cage (Figure 3A). Particle size distributions were measured with LISST-100 type B (**I**), LISST-100X type C (**III**) and LISST-HOLO (**I**) (Figures 3E and G, respectively) in the Pärnu Bay and Portmán Bay. Additional depth, salinity and temperature data were collected with the Seabird CTD (**I, III**) (Figures 3A and C). Reflectance was measured with TriOS-RAMSES instruments (e.g. Figure 3B). Water samples were collected just below the surface and at 1 m above the bottom (**II, III**) and at various depths of 1 m using Niskin bottles (**I**) (Figure 3C). Bottom sediments were collected in August in the Pärnu Bay (**III**) and Portmán Bay (**I**). Current properties and visualisation of the sediment plume were obtained from Acoustic Doppler Current Profiler (ADCP) data measured in the Portmán Bay (**I**) (Figure 3C).

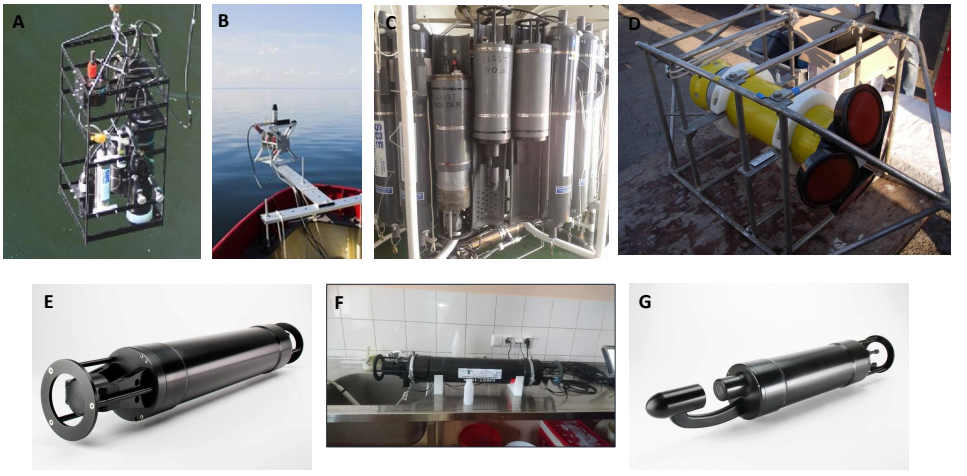

Figure 3*: Instruments used during the field campaigns: A – a cage containing WET Labs AC-S, ECO-BB3, ECO-VSF3, DH-4 datalogger and Seabird CTD, B – an above-water system of three TriOS-RAMSES hyperspectral radiometers, C – a rosette containing Niskin bottles, D – 300 kHz ADCP current profiler, E – LISST-100, F – LISST-100X in a laboratory setup, G – LISST-HOLO holographic camera*

3.3. Methodology

3.2.1. Measurement strategy

Different resuspension mechanisms were observed during the field campaigns at the four study sites where the SPM properties were investigated – Portmán, Pärnu, Haapsalu, and Matsalu bays. In the Portmán Bay, sediment plumes were triggered mechanically by trawling, and in the Estonian bays, sediments were resuspended by the natural forcing of waves and river inflows. The most complex measurement strategy was used in the Portmán Bay to generate sediment plumes. The campaign with two research vessels was conducted in two phases from 6 to 14 June 2014. The first vessel, the R/V Ramon Margalef, triggered sediment plumes by bottom trawling. The bottom trawl GOC73 (4 doors, 36 m floating line, 40 m bottom rope, 7 m side ropes) was used for the experiment, which is capable of disturbing the top 2–10 cm of sediments between or below the doors (Durrieu De Madron et al., 2005; Fiorentini, 1999). The second vessel, the R/V Ángeles Alvariño, crossed the plume perpendicularly several times with acoustic and optical instruments immediately after the trawling. The experimental setup is shown in the Figure 4. Three experiments, T1, T2, and T3 (the reference experiment), were presented in the Paper **I** (Figure 5).

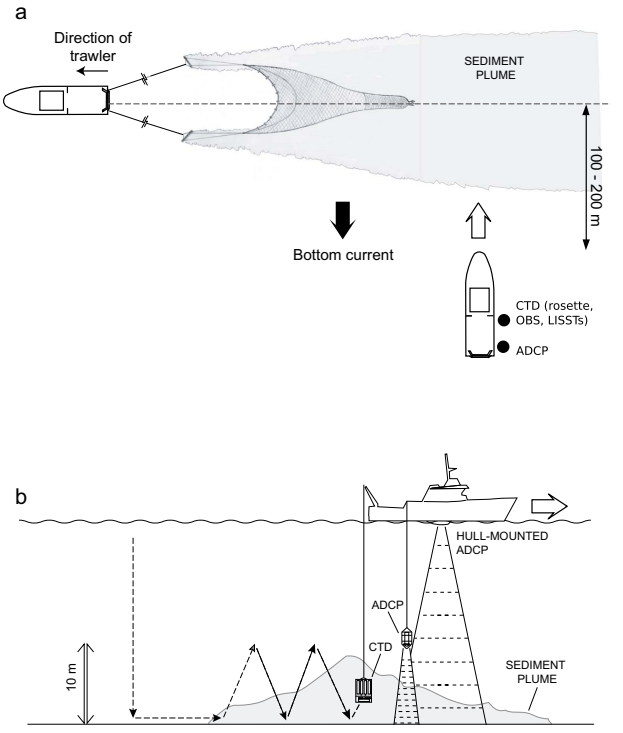

***Figure 4**: The Portman Bay experimental setup (Figure 2 from the Paper I)*

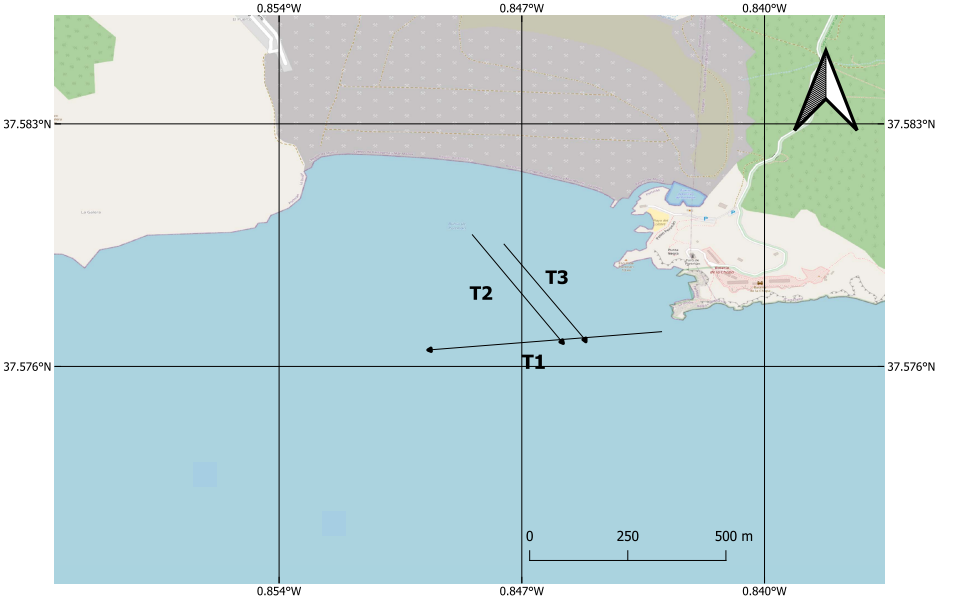

***Figure 5**: The trawling trajectories in the Portmán Bay – T3 was a reference experiment; T1 and T2 are other trawling trajectories for which the same measurements were made as for T3,*

Four campaigns were conducted in the Pärnu Bay in June 2017, April, May, and August 2018 under different conditions. The ice on the sea surface melts typically in April/early May, after which a spring bloom occurs. In July/August, depending on the weather and nutrients, a summer cyanobacterial bloom occurs. In both cases, the phytoplankton species present are not the same. The influence of the river on the water optics also differs from spring to summer. Runoff increases with snowmelt and rain in spring, and more CDOM is imported into the bay. Strong winds occur throughout the year providing a high concentration of resuspended sediments in the bay. These conditions were recorded during the August field campaign. Vertical profiles of inherent optical properties were measured at five stations in June, April, and May and at seven stations in August (see the Figure 6 and the Table 1 in the Paper III).

IOPs were also measured in the Haapsalu and Matsalu bays in July 2012, July 2013, May, September, October 2016 and July 2018. The locations of the measuring stations are shown in the Figure 6, and the details of the measured data are in the Table 1 in the Paper III.

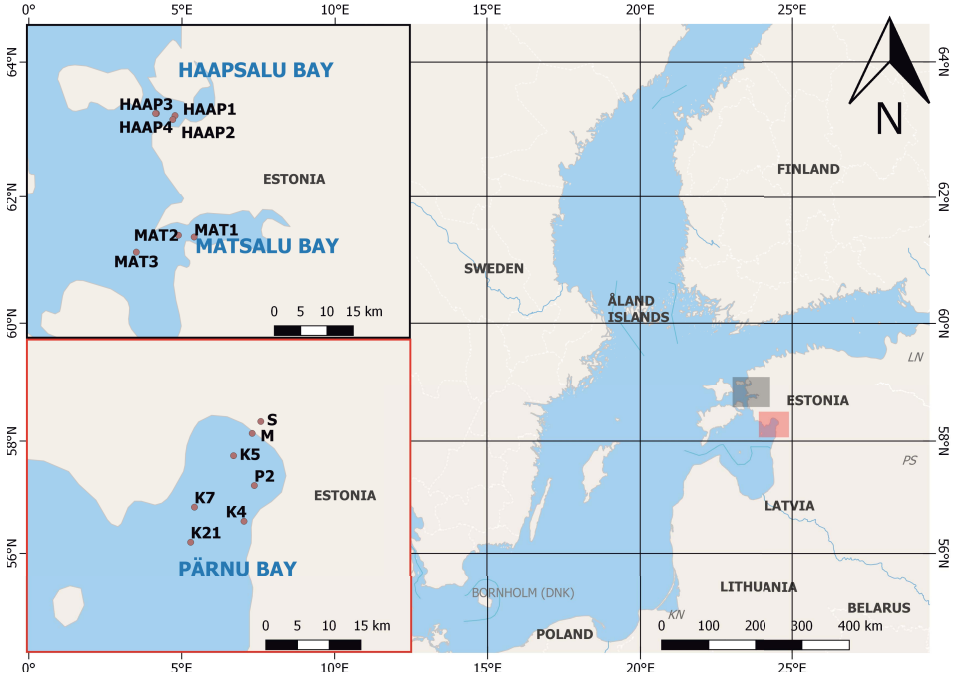

***Figure 6**: Locations of the measurement stations of the Haapsalu, Matsalu and Pärnu bays*

3.2.2. Sediment plumes geometry

A self-contained 300 kHz RDI® BB ADCP was deployed 10 metres above the bottom in the Portmán Bay to investigate the plumes triggered by bottom trawling. The profiles of current velocity and direction were measured in 20 cm-depth cells at a maximum sampling rate of 1 Hz (**I**). In addition, a WET Labs® Fluorescence and Nephelometric Turbidity Unit (FLNTU) sensor was mounted on the Seabird® 911 Plus CTD (conductivity, temperature, and depth) sensor to collect turbidity measurements calibrated against gravimetric measurements. Thus, turbidity measurements were converted to SPM concentrations ($mg \cdot l^{-1}$) using a linear equation (Eq. 1 in the Paper **I**). ADCP measures the acoustic intensity back-scattered from the moving particles. After processing the signal (see details in the Paper **I**, chapter "Acoustic characterisation of bottom trawling-triggered sediment plume"), the acoustic intensity is directly proportional to SPM concentrations (Poerbandono & Mayerle, 2004).

3.2.3. Measurement of water constituents

SPM concentrations in the Portmán Bay and Estonian bays were determined gravimetrically from Whatman GF/F filters (**I, II, III**). Suspended organic and mineral matter (SPOM and SPIM, respectively) were estimated from SPM in Estonian samples. The filters were weighed before and after combustion. After combustion at 550 °C for 30 minutes, SPOM was eliminated, which allowed the calculation of the concentrations of SPIM and SPOM (ESS, 1993). The water sample was filtered through Whatman® GF/F filters to measure the Chl-a content. Chl-a pigments were extracted with 5 mL of 96% ethanol and measured using Perkin ELMER® Lambda 35 UV/VIS or Hitachi® U-3010 UV/VIS spectro-photometers, depending on the fieldwork. Concentrations were calculated according to the method developed by Jeffrey & Humphrey (1975). The filtrate of samples passed through GF/F filters was passed again through a Millipore filter with a pore size of 0.2 μm. The absorption spectra of CDOM were measured between 350 and 750 nm using two different spectrophotometers – Perkin ELMER® Lambda 35 UV/VIS and Hitachi® U-3010 UV/VIS – following the method described in the Paper **III** and Lindell et al. (1999).

3.2.4. Metal analyses

Bottom sediments in the Portmán Bay were obtained from multicore sediment samples (locations are marked with red dots in the Figure 1 in the Paper I). Metal analyses were carried out on the bottom surface sediments (Figure 1 in the Paper **I**: red dots) and water samples. Water samples were filtered through pre-weighed Millipore filters with a pore size of 0.45 μm and dried. The particles were recovered after sonication and dried. Then the particles were digested in a

PTFE (polytetrafluoroethylene) hydrothermal autoclave reactor on a hot plate in a mixture of concentrated HNO_3 and HF. Then the organic matter was mineralised in the mixture of HNO_3 and H_2O_2. The dried residues were diluted in 2% HNO_3 and then analysed by inductively coupled plasma mass spectrometry (ICP-MS). The concentrations of heavy metals were measured using this method. Five elements, Fe, Pb, As, Cd, and Zn, were selected for further analyses.

3.2.5. Inherent optical properties

The protocols for processing, calibrating and correcting the IOP data are described in detail in the Paper **III**. Spectral absorption and attenuation coefficients ($a(\lambda)$ and $c(\lambda)$, respectively) were measured as vertical profiles with the WET Labs® AC -S spectrophotometer in Estonian bays. Interpolation of the data made it possible to obtain $a(\lambda)$ and $c(\lambda)$ between 400 and 724 nm with a step of two nm. Salinity, temperature, and scattering corrections were applied to $a(\lambda)$ and $c(\lambda)$. Spectral scattering coefficients, $b(\lambda)$, were obtained by subtracting the corrected $a(\lambda)$ from $c(\lambda)$. Spectral particulate absorption coefficients, $a_p(\lambda)$, were calculated by subtracting spectral CDOM absorption coefficients, $a_{CDOM}(\lambda)$, from total spectral absorption coefficients. Specific particulate scattering coefficients ($b_p^*(\lambda)$) were calculated by dividing the particulate scattering coefficients by the specific SPM concentrations at the stations (Eq. 5 in the Paper **III**). $b_p^*(\lambda)$ were only calculated at the same wavelengths as the backscattering.

Spectral particulate backscattering coefficients ($b_{bp}(\lambda)$) were calculated from volume scattering functions measured by WET Labs® ECO -BB3 and ECO – VSF3 sensors (Eq. 6–12 in the Paper **III**). We obtained $b_{bp}(\lambda)$ at six wavelengths – 412, 470, 532, 595, 660 and 715 nm. A peak at 595 nm was observed in the $b_{bp}(\lambda)$ spectra. The instrument was recalibrated, and analysis of the data collected after calibration showed that the measurements at 595 nm could not be used. From $b_{bp}(\lambda)$, the specific backscattering coefficients $b_{bp}^*(\lambda)$ were calculated by dividing $b_{bp}(\lambda)$ by the SPM concentrations specific to the stations (Eq. 13 in the Paper **III**).

The particulate backscattering ratio ($b_{bp}/b_p(\lambda)$) shows how much light is scattered by the particles in the backward direction. The $b_{bp}/b_p(\lambda)$ was calculated by dividing the $b_{bp}(\lambda)$ by the $b_p(\lambda)$ at the corresponding wavelengths (Eq. 14 in the Paper **III**).

3.2.6. Particle size distributions

Particle size distributions were measured with Sequoia® LISST-100 type B (**I**), LISST-100X type C (**III**) or LISST-HOLO (**I**), depending on the campaign. The LISST-100 and LISST-100X instruments are submersible multi-parameter laser in situ scattering and transmissometers that measure particle size distributions (PSD) and volume concentrations. They also measure optical transmission, attenuation, pressure and temperature. Based on the theory that particles are randomly shaped (Agrawal et al., 2008), PSDs were measured in 32 logarithmically spaced

size classes between 1.25–250 µm for LISST-100 type B and 2.50–500 µm for LISST-100X type C using a solid-state diode laser at 670 nm and custom 32-ring photodiode detectors. The highest frequency of 1 Hz was used.

LISST-HOLO is a holographic camera consisting of a 4.4 µm digital camera with a resolution of 1600x1200 pixels and a solid-state diode laser at 658 nm. The captured holograms are 3-D images projected onto a 2-D surface and stored internally. The highest frequency of 0.2 Hz was used for the measurements, and the particle size classes measured by LISST-HOLO were between 20 and 2500 µm.

LISST-100 and LISST-HOLO were deployed in a cage with CTD and Niskin bottles in the Portmán Bay, and several upcasts and downcasts were measured as the instruments passed through the sediment plume (**I**). After processing the data, the PSDs measured by LISST-100 and LISST-HOLO were merged into overlapping size classes from 20 to 250 µm, giving merged spectra of the entire PSD range between 1.25 and 2500 µm.

LISST-100X was deployed in a cage with WET Labs optical instruments in the Pärnu Bay in August 2018, and a profile was measured at each station with halts at 1 m below the surface and 1 m above the bottom (**III**).

The approach of examining primary particles after treating water samples in an ultrasonic bath has already been used in some cases (e.g. Many et al., 2016). Therefore, the measurements of PSDs were carried out in the laboratory with the LISST-100X. The water samples collected in the Portmán Bay were first filtered, dried and stored (**I**). Then these filters, which contained SPM, were placed in tubes filled with MilliQ water and treated in an ultrasonic bath for five minutes, after which the PSDs were measured with the LISST-100X. Averaging ~25 measurements per sample allowed to obtain an averaged disaggregated grain size spectrum (DIGS). The same procedure was applied to the water samples from the Pärnu Bay, which were treated in an ultrasonic bath without filtering and then measured with the LISST-100X (**III**).

The grain sizes of the bottom sediments were measured as a reference for the primary particle spectra. The surface sediment core samples from the Portmán Bay were analysed with the Coulter® LS230 Laser Diffraction Particle Size Analyser after removing the organic fraction by oxidising the freeze-dried samples with 10% H_2O_2 and after mechanical shaking for 4 hours in water and sodium polyphosphate (**I**). Soil samples from the Pärnu Bay were mixed with MilliQ water and measured in the laboratory using the LISST-100X (**III**).

During the August campaign, the particles were mainly of mineral origin. Assuming that the suspended particles are of mineral origin, the PSD slopes could be derived. In that case, the PSDs can be described by a power law approximation or "Junge-type distributions", where j is a Junge exponent (Babin et al., 2003). The steeper the slopes and the higher the j values, the higher the concentration of small particles (j~3–4). The flatter the slopes and the lower the j values, the higher the concentration of coarse particles or flocs in the water (j~2) (Buonassissi & Dierssen, 2010; Junge, 1963). First, the normalised volume concentrations of the particles were calculated. Then, the volume concentrations of each size class were divided by the volume of a sphere of the same diameter to estimate the number

of particles by size class (Eq. 5 in the Paper **I**). The power laws resulting from the number of particles and the diameter are given in the Eq. 6 in the Paper **I** and the Eq. 15 in the Paper **III**.

The 50th percentile diameter with half the cumulative volume concentration (D50) was calculated to identify groups of particles in water (Qiu et al., 2016).

3.2.7. Measurement of reflectance

An above-water system with three TriOS-RAMSES hyperspectral radiometers was used in this study.

Two RAMSES ARC hyperspectral radiance sensors measured the upwelling radiance ($L_u(\lambda)$) and the downwelling radiance ($L_d(\lambda)$) in the same azimuthal plane. A RAMSES ACC irradiance sensor measured the downwelling irradiance ($Ed(0+, \lambda)$). The nadir and zenith angles of the radiance sensors were set at 40˚ (Figure 7). The spectral range of the measurement was 350–900 nm.

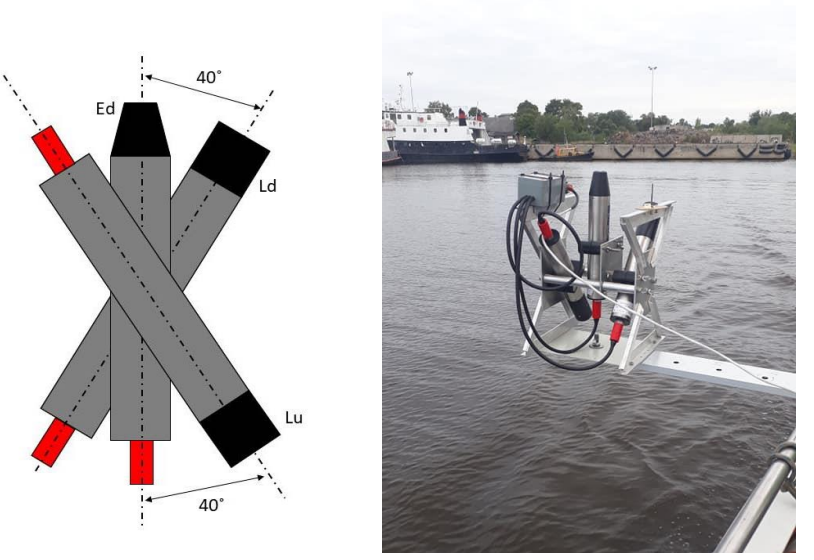

***Figure 7**: TriOS-RAMSES above-water setup*

The spectral water-leaving reflectances ($R(\lambda)$) were calculated according to the protocol of REVAMP. The radiance and irradiance spectra were linearly interpolated to a 1 nm step. Using the Eq. 1 from the Paper **II**, $R(\lambda)$ could be calculated, where $L_t = L_u$ and $L_{sky} = L_d$. Each in situ measurement station was represented by the calculated average of $R(\lambda)$ of the station.

3.2.8. Hydrolight simulations with backscattering ratios

Backscattering ratios are often used as constants in remote sensing algorithms. To better understand how variable backscattering ratios influence remote sensing reflectance, the Hydrolight 6.0 radiative transfer model was used to simulate reflectance spectra.

The constant backscattering ratio of 0.019, introduced by Kirk. (1981) for turbid waters, was tested. A backscattering ratio of 0.018 was used to see if a small change in constant influences remote sensing reflectance spectra. Then, the highest backscattering ratio from each station was used for each corresponding run. Finally, in situ measured median backscattering coefficients at five wavelengths for each station (Chpt: 3.2.5) were implemented into the model. The input for modelling contained real values of solar zenith, cloud cover, water temperature, salinity, wind speed and sun azimuthal angle relative to the wind. The water-leaving reflectance spectra were calculated between 400 and 820 nm with a 20 nm step. Semi-empirical sky model with annual average ozone value and RADTRAN-X were used. As the transparency in all the Pärnu Bay stations is low, the modelling was conducted in a water column with infinite depth. The results were compared with water-leaving reflectance spectra measured in situ with the previously described above-water measurement setup.

3.2.9. Retrieving optical water quality parameters using OWT-guided approach

As the study area is optically complex and dynamic, it was decided to use an OWT-guided approach to determine optical water quality parameters, such as the concentration of Chl-a and SPM, the absorption of CDOM at 442 nm and Secchi disc depth, from *R(λ) spectra*. This study used 132 previously published bio-optical empirical algorithms, 39 of which were used to determine SPM concentrations. The details of the algorithms are described in the Paper **II**, Appendix A, Table A1. The statistical method used to find the most appropriate algorithm for each OWT, Repeated K-fold Cross-validation, is described in detail in the Paper **II**. Subsequently, a ranking system using a combination of scaled and threshold-based statistical metrics such as Root Mean Squared Error (RMSE), Root Mean Squared Logarithmic Error (RMSLE), Mean Absolute Error (MAE), Mean Absolute Percentage Error (MAPE), Bias, R^2 and p-value allowed the selection of the best empirical algorithm for retrieving the optical water quality parameter from each OWT.

3.2.10. Satellite data

Cloud- and ice-free Sentinel-3 OLCI Level-1 full-resolution images from 2017 to 2019 were downloaded and pre-processed on the EstHub Processing Platform (Estonian Land Board's national mirror site for Copernicus satellites data and processing) (Maaamet, 2017) **(II)**. The Case-2 Regional CoastColour (C2RCC) atmospheric correction processor v1.15 was found to be the most suitable to use in this study because compared to other processors, the OWTs derived were the most accurate, and it did not over-estimate $R(\lambda)$ (Uudeberg et al., 2019). C2RCC processor was applied to all L1 images. The OWTs were assigned to the measured reflectance spectra, which in turn were convolved into OLCI bands for the Pärnu Bay case.

4. RESULTS AND DISCUSSION

4.1. Optical water type classification and predictive models for the retrieval of suspended particulate matter (SPM)

OWT-classification used in this study (Paper **II**) was introduced by Uudeberg et al. (2019). The classification was based on key reflectance spectrum characteristics measured in situ (wavelength of maximum, slope and amplitude of $R(\lambda)$). They divided boreal inland and coastal waters into five OWTs: Clear, Moderate, Turbid, Very Turbid and Brown. The spectra of Clear OWT had a maximum between 540 and 580 nm. The waters of this OWT were the most transparent and contained the lowest amounts of OAS. The spectra of Moderate OWT also had a maximum between 540 and 580 nm. The slope in the blue part was deeper in Moderate OWT, and the OAS concentration was slightly higher than in Clear OWT. The spectra of Turbid OWT had the highest maximum values of all OWT spectra. The predominant OAS in this OWT was SPM. The spectra of Very Turbid OWT had a maximum in the red region and a visible Chl-a peak showing the dominance of Chl-a. The spectra of Brown OWT had low values and a maximum in the red part of the spectrum, indicating the dominance of CDOM.

This thesis only discusses the results of the predictive models used to retrieve SPM from OLCI images. A total of 39 previously published empirical algorithms were tested. The best models for the retrieval of SPM are presented in Table 1. The model using the algorithm of Kutser et al. (2016), based on a reflectance peak at 810 nm, worked well for OLCI Moderate and Turbid OWTs with $R^2 = 0.45$ and $R^2 = 0.69$, respectively. The model used by Zhang et al. (2010), a log-transformed multiple linear regression algorithm based on a combination of *R488*, *R555*, and *R645*, was the most efficient for the Clear OWT with an $R^2 = 0.47$. Molkov et al. (2019) algorithm worked best for the Brown OWT model with an $R^2 = 0.49$. SPM concentrations obtained from the OLCI $R(\lambda)$ using the OWT approach were compared with SPM concentrations measured in situ. The correlation was good, with $R^2 = 0.79$. The Moderate OWT had the lowest coefficient of determination and tended to underestimate higher SPM concentrations.

Few previous tests of published empirical algorithms have been conducted in Estonian coastal areas. Ligi et al. (2017) found that Dekker et al. (2002) algorithm had the best correlation with in situ SPM with $R^2 = 0.29$. Toming et al. (2017) tested two SPM algorithms published by Wang et al. (2006) and Kallio et al. (2001) in the study of mapping Baltic Sea coastal waters with OLCI C2RCC processed images. These two algorithms had better correlations with in situ SPM concentrations (merged several campaigns data), $R^2 = 0.69$ and $R^2 = 0.42$, respectively. The algorithms used by both authors were also tested in the current study, but they did not qualify as the best suiting for OLCI OWTs. Compared to simple empirical models, the correlation found with the OWT-based approach was slightly better (Table 1). The best models were tested on the OWTs observed in the Pärnu Bay.

***Table 1**: The best published SPM predictive models tested in this work for each OWT and Sentinel-3 OLCI sensor. The algorithms used in these models are described in detail in the Table 1 in the Paper **II**.*

OWT	Model formula	R^2	Algorithm reference
Clear	$\log SPM = -24.36 \times R560 + 80.66 \times R665 - 1.096 \times \frac{R490}{R560} + 0.840$	0.47	Zhang et al., 2010
Moderate	$SPM = -8090.1 \times \left(R865 - \frac{R778.75 + R865}{2}\right) + 1.825$	0.45	Kutser et al., 2016
Turbid	$SPM = -7664.9 \times \left(R865 - \frac{R778.75 + R865}{2}\right) + 3.250$	0.69	Kutser et al., 2016
Very turbid	$\log SPM = -0.249 \times \log R560 + 26.20 \times R665 - 0.483 \times \log \frac{R490}{R560} + 0.095$	0.60	Tassan, 1993
Brown	$\ln SPM = 311.8 \times \left(R708.75 - \frac{R753.75 + R665}{2}\right) + 1.165$	0.49	Molkov et al., 2019

4.2. Particle dynamics in the Pärnu Bay using the OWT approach

The study of the Sentinel-3 Level-1 OLCI processed images from 2017 to 2019 with the OWT-guided approach showed that the water of the Pärnu Bay mainly belonged to the Clear, Moderate and Turbid water types, depending on the conditions in the bay (Figure 10 in the Paper **II**). In general, three conditions were observed in terms of SPM concentrations. Near the shoreline, there was always re-suspension due to wind and the shallowness of the water. When there was little river input and no wind, high SPM concentrations were recorded near the shoreline, while very little or no SPM was present in the deeper parts of the bay (Figure 8A). In this case, the OWT was generally Moderate or Turbid near the coast and Clear in the middle of the bay. Rain episodes and snowmelt were associated with higher concentrations of SPM in the river and near the river mouth (Figure 8B). The SPM was flowing out of the bay. In this case, OWT was Moderate throughout the bay, with some Clear areas in the outer part of the bay, with water near the river mouth classified as Turbid and Brown. Windy periods resulted in high concentrations of SPM throughout the bay.

As observed, the storm periods were very dynamic. On June 22, 2018, the formation of a sediment plume at the surface lasted only one day. The average wind speed was 11.2 $m \cdot s^{-1}$, and the gusts were over 21 $m \cdot s^{-1}$. The water was clear again five days after the wind episode (Figure 8C–D). With these rapid changes, the OWTs also fluctuated. Five days before and after the storm, waters near the coast were classified as Moderate, while a large area in the middle of the bay was classified as Clear. Immediately after the storm, the prevailing OWT inside the bay was Turbid and outside the bay Moderate. The study of OWTs' fluctuation showed the complexity of the water optics in the Pärnu Bay and the OWT-guided

approach's ability to obtain an estimate of SPM concentrations and dynamics compared to individual regional empirical models. Consequently, remote sensing is an excellent complement to the in situ measurements, for example, establishing time series for the area. These models depend on the optical properties of the water linked to its constituents, such as SPM.

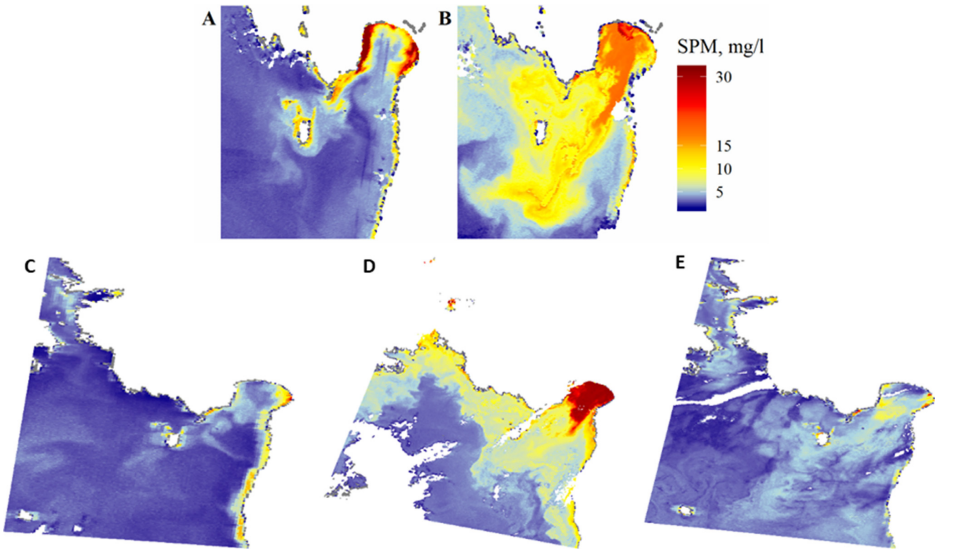

Figure 8*: The SPM concentrations in the Pärnu Bay, obtained from the water type guided approach applied on C2RCC processed Sentinel-3 OLCI Level-1 images: A – Calm conditions on 31.05.2018, B – River outflow and stronger wind conditions on 17.09.2017, C – Calm conditions six days before the storm on 17.06.2018, D – Day after the storm on 23.06.2018, E – Six days after the storm return to calm conditions on 28.06.2018*

The results obtained from the OLCI images analysis were compared with previous in situ measurements to comprehend the dynamics in concentrations of SPM better. The concentrations measured in situ after the August storm varied between 10.9 and 19.6 $mg \cdot L^{-1}$, with lower concentrations in the deeper part of the bay. These values were consistent with previous measurements. In exceptional cases, very high SPM concentrations were observed after the loading of unpacked peat at the port (> 40 $mg \cdot L^{-1}$) and due to water movement in very shallow water near the coast (~90 $mg \cdot L^{-1}$) (Lauringson, 2013; Paavel et al., 2011). Nevertheless, these amounts of SPM in the Pärnu Bay were several times lower than in more dynamic coastal areas (Mediterranean coast) and large river deltas such as the Rhone or the Amazon (largely > 100 $mg \cdot L^{-1}$ during the flood season) (Gensac et al., 2016; Ody et al., 2022). Water masses were mixed except within the river, where SPM concentrations varied considerably between the surface and bottom layers. The bottom sediment samples and previous research (Hendrikson & Ko, 2016) showed that the bottom sediment of the Pärnu Bay mainly consists of a fine layer of sand and aleurite (a sediment fraction between silt and clay: 0.004–0.063 mm) deposited on varved clay formed under ice lake conditions

before a retreating glacier. An average amount of fine particles resulted in higher concentrations of SPM than in the Portmán Bay experiment, but these concentrations were still lower than in the Gulf of Lion. The organic and inorganic components of the SPM were examined separately in the Pärnu Bay. After the storm-induced resuspension, mainly SPIM dominated the SPM. During other expeditions, the contents of SPIM and SPOM in the SPM were almost the same. As the components of the SPM have different properties and influences on the optical properties of the water, they were studied in detail, starting with the PSDs.

4.3. Particle size distributions in the Pärnu Bay after a storm

On-site PSD measurements with the LISST-100X were carried out for the first time in the Pärnu Bay in August 2018 (Paper **III**). At the time of the measurements, the water column was mixed due to waves. The spectra of PSD measured on-site and in the laboratory after sonication are shown in the Figure 9. Large particles of about 200 μm were present at all stations. Concentrations of finer particles of 20–30 μm were between 4 and 6% of the total volume concentration. In the bay, a few particles < 10 μm were present in larger quantities in stations M and S (connected to the Pärnu River). A flat mode between 3 and 50 μm was observed in stations M and S. After the sonication experiment, the particles were smaller and had a mode between 3 and 20 μm. Large particles were not present. Near the river, only particles < 10 μm were observed. The PSD of the bottom sediments consisted of a more significant amount of fine particles (< 10 μm) and a smaller amount of particles between 20 and 250 μm. The measured PSD range showed that particles of different size classes were resuspended from the bottom. Since coarse particles have a high density, they settle quickly to the bottom, and finer particles remain suspended and aggregate into flocs of > 30 μm. In order to form aggregates, the presence of cohesive fine particles such as silt, clay or organic matter is necessary in the water (Son & Hsu, 2008). Fine cohesive particles form flocs of different sizes and shapes due to their electrochemical and biological-chemical attraction. The values of D50 and *j* also confirmed the flocculation. The D50 values were smaller (6–7 μm) in the estuarine station M, and the surface station S. Inside the bay, D50 was twice as large (12–20 μm). The D50 values measured after disaggregation were < 5.20 μm. $j < 3$ were observed at the PSDs measured in the bay where aggregates formed, and $j > 3$ were observed near the river where the SPM contained a finer fraction of particles. After disaggregation, *j* was above 4 in all samples, indicating the presence of very fine particles (< 10 μm). Flocculation generally occurs in the estuaries of large rivers where there are high salinity gradients (Ody et al., 2016; Wolanskit & Gibbst, 1995) and SPM concentrations (e.g. near melting glaciers in the Arctic – Meslard et al., 2018), and in areas with a high amount of organic material (Lee et al., 2019). Zhu et al. (2018) investigated the flocculation process in low- and high-concentration sediment resuspensions with different salinity levels. He found that, with higher

salinity, organic matter and SPM concentrations, the particles' resettlement time increased, and the flocculation process occurred easily. The current study has shown that primary fine particles can form aggregates in areas with low salinity when there are mainly mineral particles and little organic material in the resuspension.

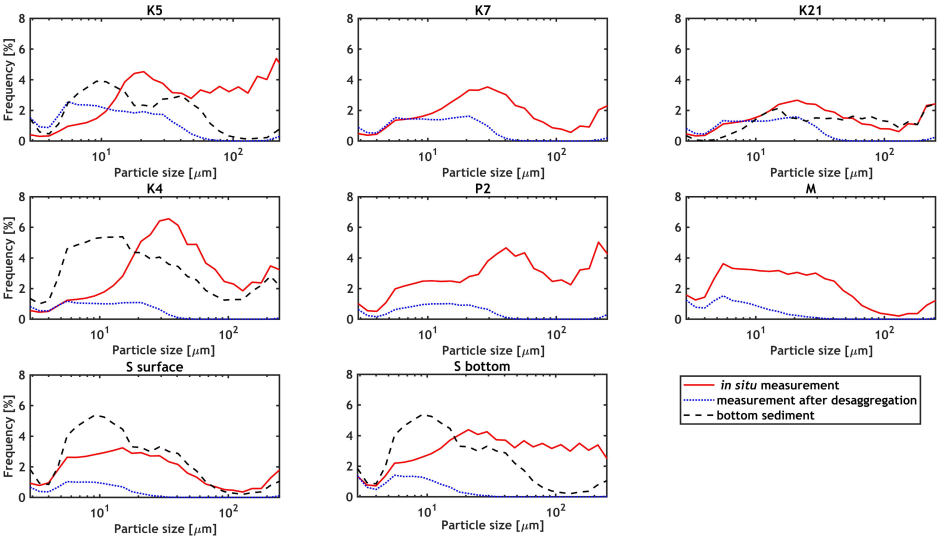

***Figure 9**: Particle size distributions (PSD) measured in the Pärnu Bay on 28.08.2018. The red line corresponds to the in situ on-site measurement, the blue line to the laboratory measurement after the sonication of the samples, and the dotted line to the bottom sample sediments' PSDs.*

4.4. Variability of the particle optical properties in Estonian coastal waters

4.4.1. Variability of IOPs

The water was generally well mixed at all times, except in the Pärnu River mouth, where the optical properties differed in the surface and bottom layers. In this study, IOPs were investigated in conjunction with suspended matter. In addition to the results of the Paper **III**, baseline spectral particulate scattering ($b_p(\lambda)$) and spectral particulate backscattering ($b_{bp}(\lambda)$) data are shown. The results indicate that the IOPs in the Pärnu Bay vary from one location to another depending on the conditions. The data presented in the figures have been merged to show the overall variability of IOPs. The detailed results of the field campaigns can be found in the Figures 4–9 in the Paper **III**.

The spectral particle absorption coefficients ($a_p(\lambda)$) varied between 0.4 and 4.69 m^{-1} in the range 424–430 nm in the Pärnu Bay (Figure 10A) and between 0.08 and 5.46 m^{-1} in the Haapsalu and Matsalu Bays (Figure 10B). The highest

$a_p(\lambda)$ were observed after the August storm and near the mouth of the river in the Pärnu Bay, indicating that the particles with high absorption came from the Pärnu River. There were absorption peaks at 675 nm, showing the presence of large amounts of Chl-a (confirmed by the concentration values around 30 mg·m^{-3}) and, thus, an algal bloom in April. The steep rises at the beginning of the $a_p(\lambda)$ spectra near the mouth of the river indicated a strong river inflow into the bay, importing large amounts of CDOM in April and May. The flux of CDOM was also confirmed by higher than average $a_{CDOM}(412)$ on these campaign days (12.65 and 14.08 m^{-1} in April and May, respectively). The $a_p(\lambda)$ was consistently lower in the outer part of the bay because the water was deep and particles did not reach the surface, and the phytoplankton growth was prevented. The $a_p(\lambda)$ showed less variability and lower values in the Haapsalu and Matsalu bays than in the Pärnu Bay. A measurement in the Haapsalu Bay showed an exception, where a visible peak occurred at 675 nm, indicating a local algal bloom.

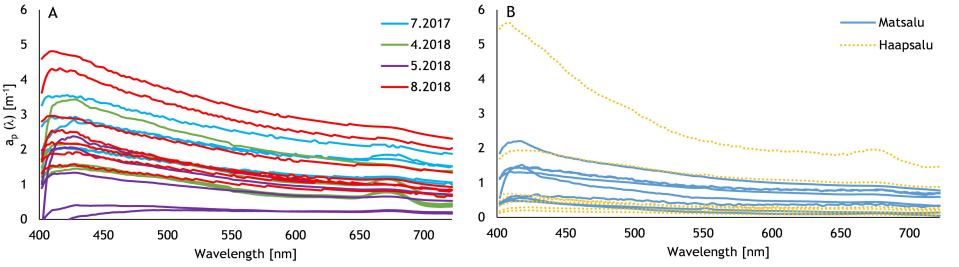

***Figure 10**: The variability of spectral particulate absorption coefficient $a_p(\lambda)$ A – in the Pärnu Bay (colours showing field campaign days) and B – in the Matsalu and Haapsalu bays (colours differentiating two bays).*

The $b_p(\lambda)$ and $b_{bp}(\lambda)$ spectra varied similarly to the $a_p(\lambda)$ spectra, which values were higher near the river mouth where the water was shallow, and the river influence was strong. They were lower near the outer part of the bay, where the water was deep. $b_p(\lambda)$ varied between 2.08 and 13.50 m^{-1} in the Pärnu Bay and between 5.00 and 13.50 m^{-1} (Figure 11A) in the Matsalu and Haapsalu Bays (Figure 11B). The maximum values of $b_{bp}(\lambda)$ were observed at 470 and 532 nm, and they varied between 0.02 and 0.23 m^{-1} in the Pärnu Bay (Figure 12A) and between 0.02 and 0.24 in the Matsalu and Haapsalu Bays (Figure 12B). There were depressions indicating the presence of phytoplankton at 675 nm in the $b_p(\lambda)$ spectra of April and in the river mouth stations of July, May and August. The highest $b_p(\lambda)$ and $b_{bp}(\lambda)$ were observed near the river mouth during the August storm due to the strong resuspension of particles from the bottom and the river inflow. The $b_p(\lambda)$ and $b_{bp}(\lambda)$ of the Haapsalu and Matsalu bays were in a similar range. The most significant variability was observed in the Haapsalu Bay, with the highest $b_p(\lambda)$ and $b_{bp}(\lambda)$ of all data.

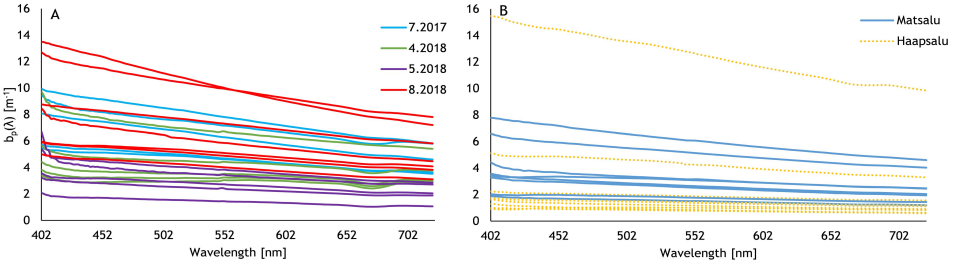

***Figure 11**: The variability of spectral particulate scattering coefficient $b_p(\lambda)$ A – in the Pärnu Bay (colours showing field campaign days) and B – in the Matsalu and Haapsalu bays (colours differentiating two bays).*

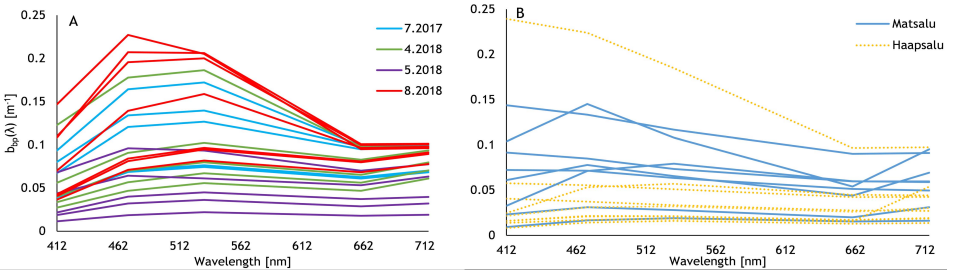

***Figure 12**: The variability of spectral particulate backscattering coefficient $b_{bp}(\lambda)$ A – in the Pärnu Bay (colours showing field campaign days) and B – in the Matsalu and Haapsalu bays (colours differentiating two bays).*

The mass-specific spectral particulate scattering coefficients ($b_p^*(\lambda)$) at 412 nm varied between 0.28 and 1.17 $m^{-2} \cdot g^{-1}$ in the Pärnu Bay (Figure 13A) and between 0.08 and 1.45 $m^{-2} \cdot g^{-1}$ in the Haapsalu and Matsalu Bays (Figure 13B). The highest $b_p^*(\lambda)$ in the Pärnu Bay was reached in July, and the lowest in May. During the storm in August and the high discharge in April, the highest $b_p^*(\lambda)$ were measured near the Pärnu River. The river did not influence particle scattering significantly in July and May because the $b_p^*(\lambda)$ inside the bay were higher than near the river.

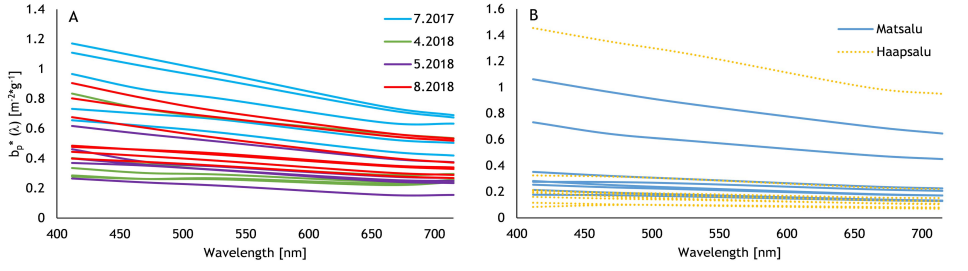

***Figure 13**: The variability of mass-specific spectral particulate scattering coefficient $b_p^*(\lambda)$ A – in the Pärnu Bay (colours showing field campaign days) and B – in Matsalu and Haapsalu bays (colours differentiating two bays).*

The mass-specific spectral particulate backscattering coefficients ($b_{bp}^*(\lambda)$) varied between 0.003 and 0.027 $m^{-2} \cdot g^{-1}$ in the Pärnu Bay (Figure 14A) and between 0.0015 and 0.023 $m^{-2} \cdot g^{-1}$ in the Haapsalu and Matsalu Bays (Figure 14B). The highest $b_{bp}^*(\lambda)$ of the Pärnu Bay was recorded in the stations in the proximity of the Pärnu River and the lowest in the outer part of the Pärnu Bay. The highest $b_{bp}^*(\lambda)$ variability was observed in the Matsalu Bay during summer. Different shapes of spectra were observed. Near the mouth of the Pärnu River, spectra with a peak at shorter wavelengths were measured. Spectra with the same shape were also measured in the Matsalu Bay. The Pärnu and Kasari rivers bring large amounts of CDOM into the Pärnu and Matsalu bays. These spectra could be due to insufficient correction of the CDOM effects on the IOPs. Nevertheless, all the corrections suggested by the manufacturer and the local CDOM corrections were applied to the data. These shapes may have been due to the presence of high quantities of CDOM. Other spectra were relatively constant or decreased with increasing wavelength.

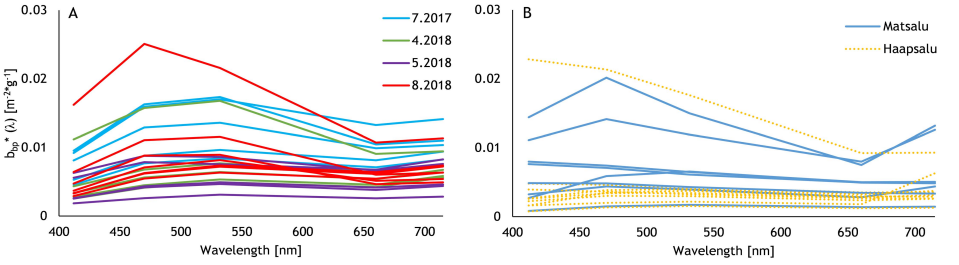

***Figure 14**: The variability of mass-specific spectral particulate backscattering coefficient $b_{bp}^*(\lambda)$ A – in the Pärnu Bay (colours showing field campaign days) and B – in the Matsalu and Haapsalu bays (colours differentiating two bays).*

4.4.2. Variability of the backscattering ratio

$b_{bp}/b_p(\lambda)$ is usually assumed to be a constant in bio-optical remote sensing algorithms but was significantly variable at study sites in the Pärnu, Haapsalu and Matsalu bays. $b_{bp}/b_p(\lambda)$ varied between 0.017 and 0.034 at the peak values in the Pärnu Bay (Figure 15A) and between 0.01 and 0.1 in the Haapsalu and Matsalu bays (Figure 15B). The detailed results of the campaigns can be found in the Figures 10 and 11 in the Paper **III**. $b_{bp}/b_p(\lambda)$ were also influenced by the location of the measurements and the weather conditions. After the storm, the highest $b_{bp}/b_p(\lambda)$ was obtained in the Pärnu Bay river station. Also, in the other measurements in the Pärnu Bay, the $b_{bp}/b_p(\lambda)$ was higher near the river mouth than in the outer parts of the bay. The spectral shape of the $b_{bp}/b_p(\lambda)$ also varied in the three bays. There were spectra with lower values at 412 nm and higher at 715 nm. The spectra with rounded shapes were observed near the river that transported large amounts of CDOM into the bay and whose effects were not sufficiently corrected,

even when the corrections suggested by the manufacturer and local CDOM corrections were applied to the data. Still, these shapes could be due to high quantities of CDOM.

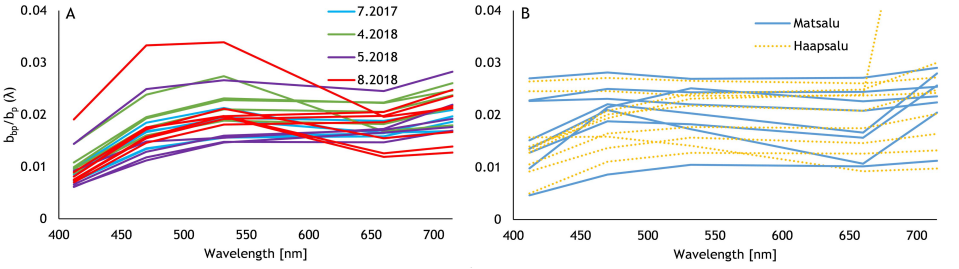

***Figure 15**: The variability of the spectral particulate backscattering ratio b_{bp}/b_p (λ) A – in the Pärnu Bay (colours showing field campaign days) and B – in the Matsalu and Haapsalu bays (colours differentiating two bays).*

$b_{bp}/b_p(\lambda)$ was also studied in relation to other properties of the particles, such as their origin and size distribution. $b_{bp}/b_p(\lambda)$ gives information about the origin of the particles. When $b_{bp}/b_p(\lambda)$ is ~0.005, the particles are generally dominated by organic matter, and when $b_{bp}/b_p(\lambda)$ is ~0.02, the particles are dominated by mineral matter (Tao et al., 2018; Ulloa et al., 1994). The $b_{bp}/b_p(\lambda)$ values were all an order of magnitude lower in our study than assumed for the dominance of organic matter, suggesting that most particles were of mineral origin. The dominance of mineral matter was supported by other analyses such as the SPOM and SPIM fractions in the SPM or the correlations between SPM, SPIM, and SPOM or between $b_{bp}/b_p(660)$, SPIM and SPOM. For example, the good correlation between $b_{bp}/b_p(660)$ and SPIM in August ($R^2 = 0.64$) showed the dominance of the mineral fraction in light backscattering. Conversely, there was a good correlation between $b_{bp}/b_p(660)$ and SPOM in May and July (R^2 = 0.66 and 0.67, respectively), indicating the dominance of the organic fraction in backscattering. However, the differentiation was not evident for some campaigns as organic and mineral material proportions were ~50/50 (e.g. in July and May). The correlation between $b_{bp}/b_p(412)$ and Chl-a was derived in April with R^2=0.98, showing the influence of phytoplankton on backscattering and the occurrence of an algal bloom.

$b_{bp}/b_p(\lambda)$ could also give clues to the particle size distributions. The smaller $b_{bp}/b_p(\lambda)$ is, the larger the particles in the assemblage and vice versa (Loisel et al., 2007; Sun et al., 2019; Xi et al., 2015). The peak values were mainly smaller within the bay, indicating the presence of coarse particles, aggregates or phytoplankton. Near the river mouth, these values were higher, indicating that the discharged particle composition consisted of finer particles. The August expedition with measured particle PSDs confirmed this assumption: within the bay, the $b_{bp}/b_p(\lambda)$ were low, and it was demonstrated that the SPM contained mainly aggregates > 30 µm. Inside the river, the $b_{bp}/b_p(\lambda)$ was an order of magnitude higher (> 0.03), and the PSDs contained finer particles as well as some aggregates.

Because the $b_{bp}/b_p(\lambda)$ is influenced by many parameters and is clearly variable due to spectral dependence, particle size distributions, and origin, it cannot be used as a constant in bio-optical remote sensing algorithms.

4.4.3. Modelling the effect of variable backscattering ratios with Hydrolight

In order to see how much $b_{bp}/b_p(\lambda)$ affects remote sensing signal, Rrs were modelled with Hydrolight radiative transfer model using different $b_{bp}/b_p(\lambda)$ and $b_b(\lambda)$. The results showed that the in situ measured reflectance spectra had the same shapes as the modelled spectra. Two tests were conducted, one with different constant $b_{bp}/b_p(\lambda)$ and one that included all measured $b_b(\lambda)$. Two cases of the Pärnu Bay data are presented in the Figure 16, the $b_{bp}/b_p(\lambda)$ spectra with higher values at shorter wavelengths (close to the Pärnu River mouth –> Figure 16A) and the $b_{bp}/b_p(\lambda)$ spectra with higher values at longer wavelengths (centre and exit of the Pärnu Bay –> Figure 16B). The results show that even when constant values with a difference of 0.001 (0.018 and 0.019, respectively) were applied to the model, the obtained Rrs spectra values changed. For the first case, the application of constant $b_{bp}/b_p(\lambda)$ had a more significant affinity with the in situ measured $R(\lambda)$ spectra shape than with the application of b_b spectra measured at five wavelengths. Hence, the highest affinity with shape and Rrs values are obtained with a constant value of $b_{bp}/b_p(\lambda)$ calculated from in situ measured $b_{bp}(532)$ and $b_p(532)$ values. For the second case (Figure 16B), only spectra obtained from $b_{bp}/b_p(\lambda)$ calculated from in situ data and b_b values measured at five wavelengths were considered in the comparison of the modelled Rrs spectra shapes with in situ $R(\lambda)$ spectrum. Even though the values of in situ spectrum are a magnitude higher than the values of modelled spectra, the shape of Rrs modelled with b_b at five wavelengths is closer to the in situ $R(\lambda)$ spectrum than the Rrs modelled with constant b_{bp}/b_p, especially near 710 nm.

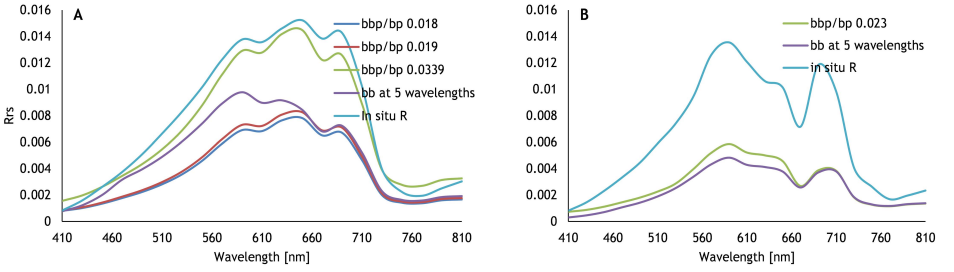

***Figure 16**: Comparison of modelled Rrs and in situ measured R(λ) spectra. Constant backscattering ratio values were used, and backscattering measured in situ at five wavelengths. These two examples are from A) Station S (August 2018, Pärnu Bay), B) Station K7 (April 2018, Pärnu Bay)*

4.5. Particle dynamics in the Portmán Bay after a trawling experiment

The use of an ADCP was another method tested for monitoring the resuspended particle concentration, dynamics and behaviour in the water column (Paper **I**). Figure 17 illustrates the geometry of the triggered plume of experiment T3. The beginning of the experiment (T0) was the moment when the doors of the trawl touched the sea bottom. The bottom was trawled for a distance of about 1000 m. During the longest experiment T3, the survey vessel crossed the generated plume up to 10 times within 4 hours before the turbidity signal disappeared. In the first three minutes, the highest concentrations of SPM were measured near the seabed (> 5 $mg \cdot L^{-1}$), and the plume extended over a distance of about 100 m and was about 5 m high. After 25 minutes, the plume was more diluted and had extended to about 100 m wide and 6 m high. 80 minutes later, the plume was diffused, and its height was reduced to 3 m. After that, the plume decreased in width and height to 2 m and reached an SPM concentration of about 2 $mg \cdot L^{-1}$. The plume disappeared after 170 minutes. The experiment showed that all the plumes produced had the highest concentrations of SPM immediately after the start of trawling, which then quickly spread, diluted and settled again. Only a tiny fraction of the particles was winnowed.

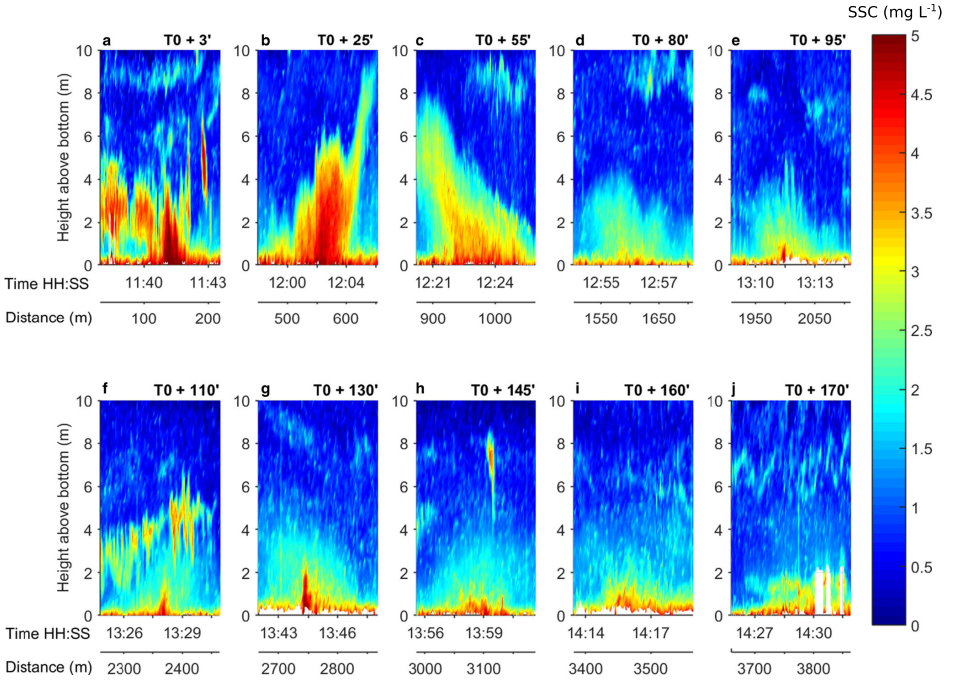

***Figure 17**: The presentation of the evolution of the triggered plume geometry (experiment T3) in the function of distance and time derived from the continuous measurements made with the ADCP instrument (Figure 5 from the Paper I)*

In a similar experiment conducted by Durrieu De Madron et al. (2005) in the Gulf of Lion, SPM concentrations were 50 $mg \cdot L^{-1}$ with a high proportion of fine particles. Therefore, it is assumed that the low particle concentration in the plumes generated in the Portmán Bay is due to the low content of fine particles in the bottom sediments.

4.6. Particle size distributions and the content of heavy metals in the generated sediment plume in the Portmán Bay

The particle size distributions measured after each crossing of the triggered sediment plume are shown in the Figure 18. Merging LISST-100 and LISST-HOLO allowed the observation of PSDs on a larger scale, between 1.25 and 1000 µm (particles > 1000 µm were absent). Immediately after trawling began, there were very high concentrations of particles larger than 500 µm (22% of the total particle assemblage). Smaller peaks were 80 (4%), 100 (6%) and 130 µm (9%). Between 25 and 55 minutes after onset, particles > 500 µm resettled and the primary mode was 100 µm with a small peak at 400 µm (< 5%).

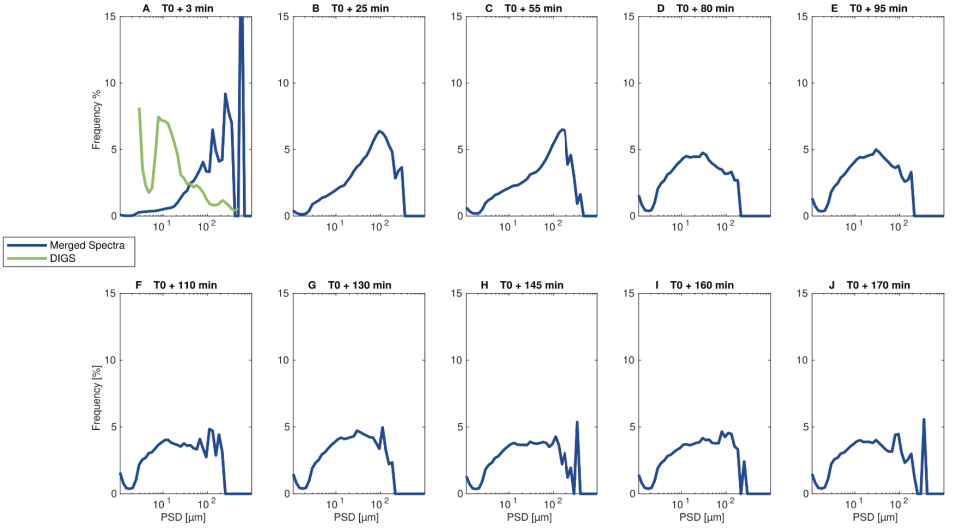

***Figure 18**: Particle size distribution (PSD) evolution during the experiment T3 of the Portmán Bay. The blue line corresponds to the merged spectra of LISST-100 and LISST-HOLO, and the green line represents disaggregated grain size spectrum (DIGS). (Figure 6 from the Paper I).*

After 80 minutes until the end of the experiment, the particles became finer. The green line in the Figure 18a shows the size distribution of the disaggregated particle assemblage size distribution. The main mode of DIGS was observed for the particles < 2 μm and the second mode for the particles of 10 μm. The calculated D50 was higher at the beginning of the experiment (46 μm) and then gradually decreased to 20 μm. The same trends were observed for *j*. The D50 values of the Pärnu Bay were three times lower than the D50 values observed at the beginning of the trawl experiment both before and after disaggregation (> 30 μm and 11 μm, respectively). Lower D50 values indicate that the bottom sediment fraction released in suspension was coarser in the Portmán Bay. The disaggregation experiment showed that the fine fraction of particles < 2 μm was resuspended, with the particles agglomerating into large flocs > 100 μm. Large particles settled quickly, and fine particles remained resuspended for at least 3 hours, extending the aquatic environment's contact time with heavy metals affiliated with particles.

Chemical analyses of the surficial bottom sediments and water samples were carried out for these experiments. Fe, Pb, As, Zn and Cd concentrations were measured in the sediments and SPM. The concentrations of these heavy metals were very high in the bottom sediments. After the start of trawling, the Fe and Pb concentrations in the SPM increased continuously, while the As and Zn values remained relatively constant throughout the experiments. The exact values can be found in the Paper **I**. The Cd values were lower than in the surface layer of bottom sediments but constant in the SPM. Heavy metals were divided into two groups. The first group contained Fe, Pb, and As. During the first hour of resuspension, the concentrations remained just below the concentrations of the bottom sediments; then, they increased. The first stage indicates the net transfer of these metals into the dissolved phase. The increase of Fe, Pb and As in the SPM during the next stage could be explained by the re-adsorption of minerals from the dissolved phase at the surface of the particles (re-adsorption of Pb and As to active Fe (oxy)hydroxide mineral phases formed in the resuspension) (Alorda-Kleinglass et al., 2019). In addition, the fine particles remained resuspended longer than large particles, suggesting that these metals have a greater affinity for small particles. Tansel & Rafiuddin. (2016) studied the concentrations of heavy metals in the Miami River sediments and found that heavy metal concentrations were 6–10 times higher in fine sediments than in coarse sediments. Fine particles incorporate heavy metals because of their large surface-to-mass ratios and significant chemical adsorptive reactions due to their mineralogy (Datta & Subramanian, 1997).

The other group contained Cd and Zn. Their concentrations remained constant throughout the experiment, indicating that trawling did not change their concentrations. It could be due to the fast dissolution of these metals in seawater. Previous studies have shown that concentrations of metals in the SPM at the end of the experiment were similar to those found in historically more polluted areas on the Barcelona coast (Palanques et al., 2017; Palanques & Diaz, 1994; Puig et al., 1999). Nevertheless, these concentrations were an order of magnitude

higher than in less polluted areas of the western Mediterranean (Heimbürger et al., 2012; Roussiez et al., 2005).

The impact of the resuspension of particles in metals on the marine environment was also estimated. A parallel experiment was conducted with mussel-covered ropes exposed to the artificially triggered metal-loaded plume (Mestre et al., 2017). Mussels are filter-feeders, which feed on marine particles suspended in the water column. Phytoplankton can be affected by metals dissolved in the water. The authors did not find a significant Fe, Pb, As, Cd, and Zn accumulation in the mussel tissues. The exposure time was insufficient, but it could be shown that the mussels were affected by the ecotoxicological effects of releasing chemical pollutants from the tailings of the sulphide mines.

CONCLUSIONS

The optical properties and the dynamics of the particles varied highly in time and space, indicating the variability of the particles' composition and origin of the particles regarding the conditions in the area (e.g. blooms, storms) in the Estonian coastal areas.

Hydrolight simulations showed that a fixed backscattering ratio constant could not be used in a rapidly changing environment. It is essential to collect more data to see in what range the backscattering ratios vary in different locations in order to implement correct data to remote sensing algorithms and bio-optical models.

The OWT-guided method, tested in the Pärnu Bay, allowed to accurately determine the dynamics of SPM from the OLCI reflectance spectra. Optical properties of coastal waters vary spatially and temporally in a wide range. Therefore, it is not surprising that using a single algorithm for the whole study area did not provide as good results as the OWT-guided method. A more detailed study of the particles' properties can help to improve the methods for retrieval of the suspended matter concentrations.

The OLCI images analysis with an OWT-guided approach showed that dynamics of the suspended sediment concentrations and OWTs varied highly and were impacted by continuous near-shore resuspension, the Pärnu River and wind episodes.

The flocculation process occurred in addition to previous findings in the brackish water of the Pärnu Bay (particles smaller than 10 μm agglomerated into aggregates larger than 30 μm).

In the Portmán Bay, the metal concentrations in particles and resuspended sediment concentrations remained at high level after the trawling experiment. Fe, Pb and As have higher affinity to the fine particles, that remain longer in suspension increasing the metal/sediments concentration ratio.

Generated sediment plumes expanded on the large area, and fine particles remained resuspended for over three hours. Thus, the experiment showed how far and how long the potential ecotoxic effect of disturbance impacts the environment.

This work allowed to collect detailed data on particle dynamics and properties under different conditions. This knowledge can be used to study the effects of these properties on the remote sensing signal and thus develop working regional remote sensing algorithms. There are still uncertainties regarding the spectral variability of the backscattering ratio. This study helped to collect data and additional observations of this parameter under different conditions. The flocculated and the non-flocculated particles do not have the same signal perceived by the satellite sensor. The size of the particles plays a role. Furthermore, the experiment in the Portmán Bay has shown that the approach used to study the environmental impact of the disturbance of metal-bearing sediments can be applied to the case of deep-sea mining. The current study leads to further research in remote sensing of suspended particulate matter, such as the investigating of artificial plumes and particle size distributions from space.

REFERENCES

Aas, E., Høkedal, J., & Sørensen, K. (2005). Spectral backscattering coefficient in coastal waters. *International Journal of Remote Sensing*, *26*(2), 331–343. https://doi.org/10.1080/01431160410001720324

Alorda-Kleinglass, A., Garcia-Orellana, J., Rodellas, V., Cerdà-Domènech, M., Tovar-Sánchez, A., Diego-Feliu, M., Trezzi, G., Sánchez-Quilez, D., Sanchez-Vidal, A., & Canals, M. (2019). Remobilization of dissolved metals from a coastal mine tailing deposit driven by groundwater discharge and porewater exchange. *Science of the Total Environment*, *688*, 1359–1372. https://doi.org/10.1016/j.scitotenv.2019.06.224

Babin, M., Morel, A., Fournier-Sicre, V., Fell, F., & Stramski, D. (2003). Light scattering properties of marine particles in coastal and open ocean waters as related to the particle mass concentration. *Limnology and Oceanography*, *48*(2), 843–859. https://doi.org/10.4319/lo.2003.48.2.0843

Barale, V. (2008). The European Marginal and Enclosed Seas: An Overview. In V. Barale & M. Gade (Eds.), *Remote Sensing of the European Seas* (pp. 3–22). Springer. https://doi.org/10.1007/978-1-4020-6772-3_1

Berthon, J. F., & Zibordi, G. (2010). Optically black waters in the northern Baltic Sea. *Geophysical Research Letters*, *37*(9), 1–6. https://doi.org/10.1029/2010GL043227

Bianchi, T. S., Engelhaupt, E., Westman, P., Andrén, T., Rolff, C., & Elmgren, R. (2000). Cyanobacterial blooms in the Baltic Sea: Natural or human-induced? *Limnology and Oceanography*, *45*(3), 716–726. https://doi.org/10.4319/lo.2000.45.3.0716

Biswas, A. K., & Tortajada, C. (2019). Water quality management: a globally neglected issue. *International Journal of Water Resources Development*, *35*(6), 913–916. https://doi.org/10.1080/07900627.2019.1670506

Bordenave, P., Delmas, F., Laplana, R., & Vernier, F. (2020). *Agriculture in coastal areas : environmental issues, impacts and regulation tools*. https://hal.inrae.fr/hal-02594849

Boss, E., Pegau, W. S., Lee, M., Twardowski, M., Shybanov, E., & Korotaev, G. (2004). Particulate backscattering ratio at LEO 15 and its use to study particle composition and distribution. *Journal of Geophysical Research*, *109*, 1–10. https://doi.org/10.1029/2002JC001514

Buonassissi, C. J., & Dierssen, H. M. (2010). A regional comparison of particle size distributions and the power law approximation in oceanic and estuarine surface waters. *Journal of Geophysical Research: Oceans*, *115*(10), 1–12. https://doi.org/10.1029/2010JC006256

Capuzzo, E., Stephens, D., Silva, T., Barry, J., & Forster, R. M. (2015). Decrease in water clarity of the southern and central North Sea during the 20th century. *Global Change Biology*, *21*(6), 2206–2214. https://doi.org/10.1111/gcb.12854

Chami, M., Shybanov, E. B., Churilova, T. Y., Khomenko, G. A., Lee, M. E., Martynov, O. V, Berseneva, G. A., & Korotaev, G. K. (2005). Optical properties of the particles in the Crimea coastal waters (Black Sea). *Journal of Geophysical Research*, *110*, 1–17. https://doi.org/10.1029/2005JC003008

Chen, C., Kong, M., Wang, Y. Y., Shen, Q. S., Zhong, J. C., & Fan, C. X. (2020). Dredging method effects on sediment resuspension and nutrient release across the sediment-water interface in Lake Taihu, China. *Environmental Science and Pollution Research International*, *27*(21), 25861–25869. https://doi.org/10.1007/S11356-019-06192-W

Coble, P. G. (2007). Marine optical biogeochemistry: The chemistry of ocean color. *Chemical Reviews*, *107*(2), 402–418. https://doi.org/10.1021/cr050350+

Conesa, H. M., Schulin, R., & Nowack, B. (2008). Mining landscape: A cultural tourist opportunity or an environmental problem?. The study case of the Cartagena-La Unión Mining District (SE Spain). *Ecological Economics*, *64*(4), 690–700. https://doi.org/10.1016/j.ecolecon.2007.06.023

Copernicus. (n.d.). *Copernicus*. https://www.copernicus.eu/en/about-copernicus/copernicus-detail (accessed on 15.09.22)

Datta, D. K., & Subramanian, V. (1997). Texture and mineralogy of sediments from the Ganges-Brahmaputra-Meghna river system in the Bengal Basin, Bangladesh and their environmental implications. *Environmental Geology*, *30*(3–4), 181–188. https://doi.org/10.1007/s002540050145

Davies-Colley, R. ., & Smith, D. . (2002). Turbidity, Suspended Sediments, and Water Clarity: A Review. *Journal of the American Water Resources Association*, *37*(5), 1085–1101.

Dekker, A. G., Vos, R. J., & Peters, S. W. M. (2002). Analytical algorithms for lake water tsm estimation for retrospective analyses of tm and spot sensor data. *International Journal of Remote Sensing*, *23*(1), 15–35. https://doi.org/10.1080/01431160010006917

Duckey, T., Lewis, M., & Chang, G. (2006). Optical oceanography: Recent advances and future directions using global remote sensing and in situ observations. *Reviews of Geophysics*, *44*(1), 1–39. https://doi.org/10.1029/2003RG000148

Durrieu De Madron, X., Ferré, B., Le Corre, G., Grenz, C., Conan, P., Pujo-Pay, M., Buscail, R., & Bodiot, O. (2005). Trawling-induced resuspension and dispersal of muddy sediments and dissolved elements in the Gulf of Lion (NW Mediterranean). *Continental Shelf Research*, *25*(19–20), 2387–2409. https://doi.org/10.1016/j.csr.2005.08.002

EEA. (2015). *The European environment – state and outlook 2015: synthesis report*. https://doi.org/10.2800/944899

EOSDIS. (n.d.). *Rrs*. https://oceancolor.gsfc.nasa.gov/atbd/rrs/ (accessed on 23.11.22)

Erftemeijer, P. L. A., Riegl, B., Hoeksema, B. W., & Todd, P. A. (2012). Environmental impacts of dredging and other sediment disturbances on corals: A review. *Marine Pollution Bulletin*, *64*(9), 1737–1765. https://doi.org/10.1016/j.marpolbul.2012.05.008

Erftemeijer, P. L. A., & Robin Lewis, R. R. (2006). Environmental impacts of dredging on seagrasses: A review. *Marine Pollution Bulletin*, *52*(12), 1553–1572. https://doi.org/10.1016/j.marpolbul.2006.09.006

ESA. (n.d.-a). *MERIS*. https://earth.esa.int/eogateway/instruments/meris (accessed on 14.06.22)

ESA. (n.d.-b). *Sentinel-3*. https://sentinels.copernicus.eu/web/sentinel/missions/sentinel-3 (accessed on 13.09.22)

ESS. (1993). ESS Method 340.2. Total suspended solids, mass balance (dried at 103–105º C), volatile suspended solids (Ignited at 550º C). *Environmental Sciences Section*, 189–192. http://www.cyanopros.com/refs/epa_TSS.pdf

Fan, X., Zhang, L., Yuan, L., Guo, B., Zhang, Q., & Huang, H. (2022). Urbanization and water quality dynamics and their spatial correlation in coastal margins of mainland China. *Ecological Indicators*, *138*(March), 108812. https://doi.org/10.1016/j.ecolind.2022.108812

Fiorentini, L. (1999). Efficiency of the bottom trawl used for the Mediterranean international trawl survey (MEDITS)Efficacité du chalut de fond utilisé pour le programme international d'évaluation des ressources halieutiques de Méditerranée (MEDITS). *Aquatic Living Resources*, *12*(3), 187–205. https://doi.org/10.1016/s0990-7440(00)88470-3

Freda, W. (2012). Spectral dependence of the correlation between the backscattering coefficient and the volume scattering function measured in the southern Baltic Sea. *Oceanologia*, *54*(3), 355–367. https://doi.org/10.5697/oc.54-3.355

Gensac, E., Martinez, J. M., Vantrepotte, V., & Anthony, E. J. (2016). Seasonal and interannual dynamics of suspended sediment at the mouth of the Amazon river: The role of continental and oceanic forcing, and implications for coastal geomorphology and mud bank formation. *Continental Shelf Research*, *118*, 49–62. https://doi.org/10.1016/j.csr.2016.02.009

Gómez-García, C., Martin-Hernandez, F., López García, J. Á., Martínez-Pagán, P., Manteca, J. I., & Carmona, C. (2015). Rock magnetic characterization of the mine tailings in Portman Bay (Murcia, Spain) and its contribution to the understanding of the bay infilling process. *Journal of Applied Geophysics*, *120*, 48–59. https://doi.org/10.1016/j.jappgeo.2015.06.008

Hannington, M., Jamieson, J., Monecke, T., Petersen, S., & Beaulieu, S. (2011). The abundance of seafloor massive sulfide deposits. *Geology*, *39*(12), 1155–1158. https://doi.org/10.1130/G32468.1

Hayes, D. F., Crockett, T. R., Ward, T. J., & Averett, D. (2000). Sediment Resuspension during Cutterhead Dredging Operations. *Journal of Waterway, Port, Coastal, and Ocean Engineering*, *126*(3), 153–161. https://doi.org/10.1061/(asce)0733-950x(2000)126:3(153)

Hecht, T., & van der Lingen, C. D. (1992). Turbidity-induced changes in feeding strategies of fish in estuaries. *South African Journal of Zoology*, *27*(3), 95–107. https://doi.org/10.1080/02541858.1992.11448269

Heimbürger, L. E., Cossa, D., Thibodeau, B., Khripounoff, A., Mas, V., Chiffoleau, J. F., Schmidt, S., & Migon, C. (2012). Natural and anthropogenic trace metals in sediments of the Ligurian Sea (Northwestern Mediterranean). *Chemical Geology*, *291*, 141–151. https://doi.org/10.1016/j.chemgeo.2011.10.011

Hein, J. R., Mizell, K., Koschinsky, A., & Conrad, T. A. (2013). Deep-ocean mineral deposits as a source of critical metals for high- and green-technology applications: Comparison with land-based resources. *Ore Geology Reviews*, *51*, 1–14. https://doi.org/10.1016/j.oregeorev.2012.12.001

Hendrikson&Ko. (2016). *Pärnu maakonnaga piirneva mereala maakonnaplaneering II köide*. https://maakonnaplaneering.ee/documents/2845826/18607509/4_KSH+aruanne.pdf/3a8f5781-2909-4d32-8a63-5f6e672503df

Hettige, N., Weerasekara, K., Azmy, S., & Jinadasa, K. (2014). Water Pollution in Selected Coastal Areas in Western Province, Sri Lanka: A Baseline Survey. *Journal of Environmental Professionals Sri Lanka*, *3*(2), 12. https://doi.org/10.4038/jepsl.v3i2.7843

Hirabayashi, Y., Alifu, H., Yamazaki, D., Imada, Y., Shiogama, H., & Kimura, Y. (2021). Anthropogenic climate change has changed frequency of past flood during 2010-2013. *Progress in Earth and Planetary Science*, *8*(1). https://doi.org/10.1186/s40645-021-00431-w

Hunter, P. D., Tyler, A. N., Carvalho, L., Codd, G. A., & Maberly, S. C. (2010). Hyperspectral remote sensing of cyanobacterial pigments as indicators for cell populations and toxins in eutrophic lakes. *Remote Sensing of Environment*, *114*(11), 2705–2718. https://doi.org/10.1016/j.rse.2010.06.006

Jeffrey, S. W., & Humphrey, G. F. (1975). New spectrophotometric equations for determining chlorophylls a, b, c1 and c2 in higher plants, algae and natural phytoplankton. *Biochemie Und Physiologie Der Pflanzen*, *167*(2), 191–194. https://doi.org/10.1016/S0015-3796(17)30778-3

Junge, C. E. (1963). *Air Chemistry and Radioactivity*. Academic Press.

Kahru, Mati, Bittig, H., Elmgren, R., Fleming, V., Lee, Z., & Rehder, G. (2022). Baltic Sea transparency from ships and satellites: centennial trends. *Marine Ecology Progress Series*, *697*, 1–13. https://doi.org/10.3354/meps14151

Kahru, Matti, Horstmann, U., & Rud, O. E. (1994). [PDF] Satellite detection of increased cyanobacteria blooms in the Baltic Sea: Natural fluctuation or ecosystem change? | Semantic Scholar. *Ambio*, *23*(8), 469–472. https://www.semanticscholar.org/paper/Satellite-detection-of-increased-cyanobacteria-in-Kahru-Horstmann/ee64147087bed1a9331d06cef506a757022955d0

Kako, T., Ichihara, F., Liu, G., Meng, X., & Ye, J. (2019). Study on the enhancement of photocatalytic environment purification through ubiquitous-red-clay loading. *SN Applied Sciences*, *1*(1), 1–8. https://doi.org/10.1007/s42452-018-0149-x

Kallio, K., Kutser, T., Hannonen, T., Koponen, S., Pulliainen, J., Vepsäläinen, J., & Pyhälahti, T. (2001). Retrieval of water quality from airborne imaging spectrometry of various lake types in different seasons. *Science of the Total Environment*, *268*(1–3), 59–77. https://doi.org/10.1016/S0048-9697(00)00685-9

Kirk, J. (2011). *Light and Photosynthesis in Aquatic Ecosystems*. Cambridge University Press.

Kirk, J. T. (1981). Estimation of the scattering coefficient of natural waters using underwater irradiance measurements. *Australian Journal of Marine and Freshwater Research*, *32*, 533–539.

Klais, R., Tamminen, T., Kremp, A., Spilling, K., & Olli, K. (2011). Decadal-scale changes of Dinoflagellates and Diatoms in the Anomalous Baltic Sea spring bloom. *PLoS ONE*, *6*(6). https://doi.org/10.1371/journal.pone.0021567

Kotta, J., Jaanus, A., & Kotta, I. (2008). Haapsalu and Matsalu Bays. In U. Schiewer (Ed.), *Ecology of Bltic Coastal Waters. Ecological Studies, vol 197* (pp. 245–258). Springer, Berlin. https://doi.org/10.1007/978-3-540-73524-3_11

Kotta, J., Lauringson, V., Martin, G., Simm, M., Kotta, I., Herkül, K., & Ojaveer, H. (2008). Gulf of Riga and Pärnu Bay. In U. Schiewer (Ed.), *Ecology of the Baltic Coastal Waters. Ecological studies, vol.197* (Issue January, pp. 217–243). Springer Berlin. https://doi.org/10.1007/978-3-540-73524-3_10

Kowalczuk, P. (1999). Seasonal variability of yellow substance absorption in the surface layer of the Baltic Sea. *Journal of Geophysical Research: Oceans*, *104*(C12), 30047–30058. https://doi.org/10.1029/1999jc900198

Kratzer, S., & Moore, G. (2018). Inherent optical properties of the Baltic Sea in comparison to other seas and oceans. *Remote Sensing*, *10*(3). https://doi.org/10.3390/rs10030418

Kutser, T., Paavel, B., Metsamaa, L., & Vahtmä, E. (2009). Mapping coloured dissolved organic matter concentration in coastal waters. *International Journal of Remote Sensing*, *30*(22), 5843–5849. https://doi.org/10.1080/01431160902744837

Kutser, Tiit, Hiire, M., Metsamaa, L., Vahtmäe, E., Paavel, B., & Aps, R. (2009). Field measurements of spectral backscattering coefficient of the Baltic Sea and boreal lakes. *Boreal Environment Research*, *14*(2), 305–312.

Kutser, Tiit, Paavel, B., Verpoorter, C., Ligi, M., Soomets, T., Toming, K., & Casal, G. (2016). Remote Sensing of Black Lakes and Using 810 nm Reflectance Peak for Retrieving Water Quality Parameters of Optically Complex Waters. *Remote Sensing*, *8*(497), 1–15. https://doi.org/10.3390/rs8060497

Lauringson, V. (2013). *Pärnu lahe seisundi parandamine tehislike riffide abil 1 . etapp* (Issue 878). https://www.kik.ee/sites/default/files/878.pdf

Lee, B. J., Kim, J., Hur, J., Choi, I. H., Toorman, E. A., Fettweis, M., & Choi, J. W. (2019). Seasonal Dynamics of Organic Matter Composition and Its Effects on Suspended Sediment Flocculation in River Water. *Water Resources Research*, *55*(8), 6968–6985. https://doi.org/https://doi.org/10.1029/2018WR024486

Ligi, M., Kutser, T., Kallio, K., Attila, J., Koponen, S., Paavel, B., Soomets, T., & Reinart, A. (2017). Testing the performance of empirical remote sensing algorithms in the Baltic Sea waters with modelled and in situ reflectance data. *Oceanologia*, *59*(1), 57–68. https://doi.org/10.1016/j.oceano.2016.08.002

Lindell, T., Pierson, D., Premazzi, G., & Zilioti, E. (1999). *Manual for monitoring European lakes using remote sensing techniques*.

Loisel, H., Mériaux, X., Berthon, J. F., & Poteau, A. (2007). Investigation of the optical backscattering to scattering ratio of marine particles in relation to their biogeochemical composition in the eastern English Channel and southern North Sea. *Limnology and Oceanography*, *52*(2), 739–752. https://doi.org/10.4319/lo.2007.52.2.0739

Maaamet. (2017). *ESTHub Processing Platform*. https://ehcalvalus.maaamet.ee/calest/calvalus.jsp (accessed on 13.06.22)

Manteca, J. I., García, J. Á. L., Oyarzun, R., & Carmona, C. (2014). The beach placer iron deposit of Portman Bay, Murcia, SE Spain: The result of 33 years of tailings disposal (1957–1990) to the Mediterranean seaside. *Mineralium Deposita*, *49*(6), 777–783. https://doi.org/10.1007/s00126-014-0511-x

Many, G., Bourrin, F., Durrieu de Madron, X., Pairaud, I., Gangloff, A., Doxaran, D., Ody, A., Verney, R., Menniti, C., Le Berre, D., & Jacquet, M. (2016). Particle assemblage characterization in the Rhone River ROFI. *Journal of Marine Systems*, *157* (January), 39–51. https://doi.org/10.1016/j.jmarsys.2015.12.010

Martín, J., Puig, P., Palanques, A., & Ribó, M. (2014). Trawling-induced daily sediment resuspension in the flank of a Mediterranean submarine canyon. *Deep-Sea Research Part II: Topical Studies in Oceanography*, *104*, 174–183. https://doi.org/10.1016/j.dsr2.2013.05.036

Martinez-Frias, J. (1997). Mine waste pollutes Mediterranean [1]. *Nature*, *388*(6638), 120. https://doi.org/10.1038/40506

Mas, J. F., & Flores, J. J. (2008). The application of artificial neural networks to the analysis of remotely sensed data. *International Journal of Remote Sensing*, *29*(3), 617–663. https://doi.org/10.1080/01431160701352154

Masas de agua costeras. (n.d.). https://www.chsegura.es/en/cuenca/caracterizacion/masas-de-agua-superficiales/masas-de-agua-costeras.html (accessed on 14.11.22)

Mateo-Sagasta, J., Zadeh, S. ., Turral, H., & Burke, J. (2017). Water Pollution from Agriculture: A Global Review. In *The Food and Agricultural Organization.*

Matthews, M. W., & Matthews, M. W. (2011). *A current review of empirical procedures of remote sensing in inland and near-coastal transitional waters*. *1161*. https://doi.org/10.1080/01431161.2010.512947

Mckee, D., & Cunningham, A. (2005). scattering phase function and its implication for modeling radiance transfer in shelf seas. *Applied Optics*, *44*(1), 126–135.

McMurtry, G. M. (2019). Deep-Sea Sediment: Authigenic Deposits. *Encyclopedia of Ocean Sciences*, 121–132. https://doi.org/10.1016/B978-0-12-409548-9.11645-8

Mengual, B., Cayocca, F., Le Hir, P., Draye, R., Laffargue, P., Vincent, B., & Garlan, T. (2016). Influence of bottom trawling on sediment resuspension in the 'Grande-Vasière' area (Bay of Biscay, France). *Ocean Dynamics*, *66*(9), 1181–1207. https://doi.org/10.1007/s10236-016-0974-7

Meslard, F., Bourrin, F., Many, G., & Kerhervé, P. (2018). Suspended particle dynamics and fluxes in an Arctic fjord (Kongsfjorden, Svalbard). *Estuarine, Coastal and Shelf Science*, *204*, 212–224. https://doi.org/10.1016/j.ecss.2018.02.020

Mestre, N. C., Rocha, T. L., Canals, M., Cardoso, C., Danovaro, R., Dell'Anno, A., Gambi, C., Regoli, F., Sanchez-Vidal, A., & Bebianno, M. J. (2017). Environmental hazard assessment of a marine mine tailings deposit site and potential implications for deep-sea mining. *Environmental Pollution*, *228*, 169–178. https://doi.org/10.1016/j.envpol.2017.05.027

Miller, K. A., Thompson, K. F., Johnston, P., & Santillo, D. (2018). An overview of seabed mining including the current state of development, environmental impacts, and knowledge gaps. *Frontiers in Marine Science*, *4*(JAN). https://doi.org/10.3389/fmars.2017.00418

Mobley, C. D. (1994). Optical Properties of Water. In *Light and Water: Radiative Transfer in Natural Waters* (pp. 60–142). Academic Press.

Mobley, C. D. (2022a). Atmospheric correction. In C. D. Mobley (Ed.), *The Ocean Optics Book* (pp. 529–596). International Ocean Colour Coordinating Group (IOCCG). https://doi.org/10.25607/OBP-1710

Mobley, C. D. (2022b). Optical Constituents of the Ocean. In C. D. Mobley (Ed.), *The Oceanic Optics Book* (p. 924). International Ocean Colour Coordinating Group (IOCCG). https://doi.org/10.25607/OBP-1710

Molkov, A. A., Fedorov, S. V., Pelevin, V. V., & Korchemkina, E. N. (2019). Regional models for high-resolution retrieval of chlorophyll a and TSM concentrations in the Gorky Reservoir by Sentinel-2 imagery. *Remote Sensing*, *11*(10). https://doi.org/10.3390/rs11101215

Morel, A., & Prieur, L. (1977). Analysis of variations in ocean color. *Limnology and Oceanography*, *22*(4), 709–722. https://doi.org/10.4319/lo.1977.22.4.0709

Ody, A., Doxaran, D., Vanhellemont, Q., Nechad, B., Novoa, S., Many, G., Bourrin, F., Verney, R., Pairaud, I., & Gentili, B. (2016). Potential of high spatial and temporal ocean color satellite data to study the dynamics of suspended particles in a micro-tidal river plume. *Remote Sensing*, *8*(3). https://doi.org/10.3390/rs8030245

Ody, A., Doxaran, D., Verney, R., Bourrin, F., Morin, G. P., Pairaud, I., & Gangloff, A. (2022). Ocean Color Remote Sensing of Suspended Sediments along a Continuum from Rivers to River Plumes: Concentration, Transport, Fluxes and Dynamics. *Remote Sensing*, *14*(9), 1–37. https://doi.org/10.3390/rs14092026

Ohde, T., Siegel, H., & Gerth, M. (2007). Validation of MERIS Level-2 products in the Baltic Sea, the Namibian coastal area and the Atlantic Ocean. *International Journal of Remote Sensing*, *28*(3–4), 609–624. https://doi.org/10.1080/01431160600972961

Paavel, B., Arst, H., Metsamaa, L., Toming, K., & Reinart, A. (2011). Optical investigations of CDOM-rich coastal waters in Pärnu Bay. *Estonian Journal of Earth Sciences*, *60*(2), 102–112. https://doi.org/10.3176/earth.2011.2.04

Palanques, A., & Diaz, J. I. (1994). Anthropogenic heavy metal pollution in the sediments of the Barcelona continental shelf (Northwestern Mediterranean). *Marine Environmental Research*, *38*(1), 17–31. https://doi.org/10.1016/0141-1136(94)90043-4

Palanques, A., Lopez, L., Guillén, J., Puig, P., & Masqué, P. (2017). Decline of trace metal pollution in the bottom sediments of the Barcelona City continental shelf (NW Mediterranean). *Science of the Total Environment*, *579*, 755–767. https://doi.org/10.1016/j.scitotenv.2016.11.031

Peña, J. A., Manteca, J. I., Martínez-Pagán, P., & Teixidó, T. (2013). Magnetic gradient map of the mine tailings in Portman Bay (Murcia, Spain) and its contribution to the understanding of the bay infilling process. *Journal of Applied Geophysics*, *95*, 115–120. https://doi.org/10.1016/j.jappgeo.2013.05.011

Poerbandono, & Mayerle, R. (2004). Assessment of Approaches for Converting Acoustic Echo Intensity into Suspended Sediment Concentration. *Hydrography*, 1–13.

Pozdnyakov, D., & Graßl, H. (2003). *Color of Inland and Coastal Waters: A Methodology for its Interpretation* (A. Lang (Ed.)). Springer Berlin.

Prieur, L. (1981). Louis Prieur. *Limonology And Oceanography*, *26*(4), 671–689. http://www.jstor.org/stable/10.2307/2836033

Puig, P., Palanques, A., Sanchez-Cabeza, J. A., & Masqué, P. (1999). Heavy metals in particulate matter and sediments in the southern Barcelona sedimentation system (North-western Mediterranean). *Marine Chemistry*, *63*(3–4), 311–329. https://doi.org/10.1016/S0304-4203(98)00069-3

Qiu, Z., Sun, D., Hu, C., Wang, S., Zheng, L., Huan, Y., & Peng, T. (2016). Variability of particle size distributions in the Bohai Sea and the Yellow Sea. *Remote Sensing*, *8*(11). https://doi.org/10.3390/rs8110949

Roussiez, V., Ludwig, W., Probst, J. L., & Monaco, A. (2005). Background levels of heavy metals in surficial sediments of the Gulf of Lions (NW Mediterranean): An approach based on 133Cs normalization and lead isotope measurements. *Environmental Pollution*, *138*(1), 167–177. https://doi.org/10.1016/j.envpol.2005.02.004

Rowe, D. K., & Dean, T. L. (1998). Effects of turbidity on the feeding ability of the juvenile migrant stage of six New Zealand freshwater fish species. *New Zealand Journal of Marine and Freshwater Research*, *32*(1), 21–29. https://doi.org/10.1080/00288330.1998.9516803

Son, M., & Hsu, T. J. (2008). Flocculation model of cohesive sediment using variable fractal dimension. *Environmental Fluid Mechanics*, *8*(1), 55–71. https://doi.org/10.1007/s10652-007-9050-7

Soomets, T., Toming, K., Paavel, B., & Kutser, T. (2022). Evaluation of remote sensing and modeled chlorophyll-a products of the Baltic Sea. *Journal of Applied Remote Sensing*, *16*(04), 1–14. https://doi.org/10.1117/1.jrs.16.046516

Stramska, M., Stramski, D., Mitchell, B. G., & Mobley, C. D. (2000). Estimation of the absorption and backscattering coefficients from in-water radiometric measurements. *Limnology and Oceanography*, *45*(3), 628–641. https://doi.org/10.4319/lo.2000.45.3.0628

Sun, D., Su, X., Wang, S., Qiu, Z., Ling, Z., Mao, Z., & He, Y. (2019). Variability of particulate backscattering ratio and its relations to particle intrinsic features in the Bohai Sea, Yellow Sea, and East China Sea. *Optics Express*, *27*(3), 3074. https://doi.org/10.1364/oe.27.003074

Tabari, H. (2020). Climate change impact on flood and extreme precipitation increases with water availability. *Scientific Reports*, *10*(1), 1–10. https://doi.org/10.1038/s41598-020-70816-2

Tansel, B., & Rafiuddin, S. (2016). Heavy metal content in relation to particle size and organic content of surficial sediments in Miami River and transport potential. *International Journal of Sediment Research*, *31*(4), 324–329. https://doi.org/10.1016/j.ijsrc.2016.05.004

Tao, J., Hill, P. S., Boss, E. S., & Milligan, T. G. (2018). *Variability of Suspended Particle Properties Using Optical Measurements Within the Columbia River Estuary*. 6296–6311. https://doi.org/10.1029/2018JC014093

Tassan, S. (1993). An improved in-water algorithm for the determination of chlorophyll and suspended sediment concentration from Thematic Mapper data in coastal waters. *International Journal of Remote Sensing*, *14*(6), 1221–1229. https://doi.org/10.1080/01431169308904406

Tessier, A. (1992). Sorption of Trace Elements on Natural Particles in Oxic Environments. *Environmental Particles*, 425–454. https://doi.org/10.1201/9780429286223-11

Toming, K., Kutser, T., Uiboupin, R., Arikas, A., Vahter, K., & Paavel, B. (2017). Mapping water quality parameters with Sentinel-3 Ocean and Land Colour Instrument imagery in the Baltic Sea. *Remote Sensing*, *9*(10). https://doi.org/10.3390/rs9101070

Ulloa, O., Sathyendranath, S., & Platt, T. (1994). Effect of the particle-size distribution on the backscattering ratio in seawater. *Applied Optics*, *33*(20), 7070–7077.

Uudeberg, K., Ansko, I., Getter, P., & Ansper, A. (2019). Using Optical Water Types to Monitor Changes in Optically Complex Inland and Coastal Waters. *Remote Sensing*, *11(19)*(2297), 1–20. https://doi.org/10.3390/rs11192297

Van Dover, C. L. (2011). Mining seafloor massive sulphides and biodiversity: What is at risk? *ICES Journal of Marine Science*, *68*(2), 341–348. https://doi.org/10.1093/icesjms/fsq086

Wang, F., Han, L., Kung, H. T., & van Arsdale, R. B. (2006). Applications of Landsat-5 TM imagery in assessing and mapping water quality in Reelfoot Lake, Tennessee. *International Journal of Remote Sensing*, *27*(23), 5269–5283. https://doi.org/10.1080/01431160500191704

Whitmire, A. L., Boss, E., Cowles, T. J., & Pegau, W. S. (2007). Spectral variability of the particulate backscattering ratio. *Optics Express*, *15*(11), 7019–7031. https://doi.org/10.1029/2005JC003008

Wolanskit, E., & Gibbst, R. J. (1995). Flocculation of Suspended Sediment in the Fly River Estuary , Papua New Guinea. *Journal of Coastal Research*, *11*(3), 754–762.

Woźniak, Slawomir B., Meler, J., Lednicka, B., Zdun, A., & Stoń-Egiert, J. (2011). Inherent optical properties of suspended particulate matter in the southern Baltic Sea. *Oceanologia*, *53*(3), 691–729. https://doi.org/10.5697/oc.53-3.691

Woźniak, Sławomir B., Meler, J., & Stoń-Egiert, J. (2022). Inherent optical properties of suspended particulate matter in the southern Baltic Sea in relation to the concentration, composition and characteristics of the particle size distribution; new forms of multi-component parameterizations of optical properties. *Journal of Marine Systems*, *229*. https://doi.org/10.1016/j.jmarsys.2022.103720

Woźniak, Sławomir B., Sagan, S., Zabłocka, M., Stoń-Egiert, J., & Borzycka, K. (2018). Light scattering and backscattering by particles suspended in the Baltic Sea in relation to the mass concentration of particles and the proportions of their organic and inorganic fractions. *Journal of Marine Systems*, *182*(December 2017), 79–96. https://doi.org/10.1016/j.jmarsys.2017.12.005

Xi, H., Larouche, P., Michel, C., & Tang, S. (2015). Beam attenuation, scattering and backscattering of marine particles in relation to particle size distribution and composition in Hudson Bay (Canada). *Journal of Geophysical Research: Oceans*, *120*(5), 3286–3300. https://doi.org/10.1002/2014JC010668

Yang, H., Kong, J., Hu, H., Du, Y., Gao, M., & Chen, F. (2022). A Review of Remote Sensing for Water Quality Retrieval: Progress and Challenges. *Remote Sensing*, *14*(8). https://doi.org/10.3390/rs14081770

Zhang, M., Tang, J., Dong, Q., Song, Q. T., & Ding, J. (2010). Retrieval of total suspended matter concentration in the Yellow and East China Seas from MODIS imagery. *Remote Sensing of Environment*, *114*(2), 392–403. https://doi.org/10.1016/j.rse.2009.09.016

Zhu, Z., Xiong, X., Liang, C., & Zhao, M. (2018). On the flocculation and settling characteristics of low- and high-concentration sediment suspensions: effects of particle concentration and salinity conditions. *Environmental Science and Pollution Research*, *25*(14), 14226–14243. https://doi.org/10.1007/s11356-018-1668-0

Zia, H., Harris, N. R., Merrett, G. V., Rivers, M., & Coles, N. (2013). The impact of agricultural activities on water quality: A case for collaborative catchment-scale management using integrated wireless sensor networks. *Computers and Electronics in Agriculture*, *96*, 126–138. https://doi.org/10.1016/j.compag.2013.05.001

SUMMARY IN ESTONIAN

Heljumi dünaamika ja omadused optiliselt keerulistes veekogudes

Rannikualad on sotsiaalmajanduslikult olulised piirkonnad linnaarengu, turismi, transpordi, ehitustegevuse ja taastuva energia arendamiseks. Sageli halvendab intensiivne inimtegevus rannikualade veekvaliteeti, mis omakorda kahjustab vee ökosüsteemi. Aastasadu on veekogude omaduste uurimiseks kasutatud kontaktmõõtmisi, kuid viimastel aastakümnetel on kättesaadavaks muutunud ka kaugseire. Satelliidisensoritega on võimalik teostada regulaarseid mõõtmisi, kattes lühikese perioodi jooksul sama sensoriga suuri maa-alasid. Euroopa Komisjon koos Euroopa Kosmoseagentuuriga on viimastel aastatel saatnud orbiidile seeria Sentinel satelliite, millest veeseirajaid huvitavad enim Sentinel-3 seeria satelliidid, sest need on disainitud spetsiaalselt veekogude seireks. Selleks, et satelliitseire tulemused oleksid usaldusväärsed, on vaja lahendada mitu küsimust. Satelliitsensorid mõõdavad signaali, mis pärineb veekogu pinnakihist. Seda signaali mõjutavad lisaks veele optiliselt aktiivsed ained, nagu fütoplanktoni pigment klorofüll-a, heljum ja värvunud lahustunud orgaaniline aine. Käesoleva doktoritöö põhiliseks eesmärgiks oli uurida heljumi optilisi omadusi ja kontsentratsiooni dünaamikat. Heljum koosneb mineraalsetest ja orgaanilistest osakestest. Selle kontsentratsioon vees on mõjutatud inimtegevusest (nt traaleritega kalapüük, süvendustööd, ehitused rannikualadel) ja looduslikest protsessidest (nt tormid, lainetus, jõgede sissevool). Vee hägususe suurenemine heljumi kontsentratsiooni kasvu tõttu mõjutab vee valgusvälja ja seetõttu jõuab vähem valgust veekogu põhjakihtidesse. See omakorda pärsib vee elustiku toimetulekut. Rööpkalad ei näe saaki püüda, samas kalamaimud saavad rööpkalade eest lihtsamini peituda. Optilisest seisukohast on heljumi põhiomaduseks võime tugevasti valgust hajutada. Põhiliselt kehtib see mineraalse fraktsiooni kohta, sest orgaaniline fraktsioon võib päris suures osas valgust ka neelata. Valguse hajutamine sõltub heljumi suurusjaotusest, päritolust ja kujust. Mida väiksemad on heljumi osakesed, seda paremini nad hajutavad valgust erinevates suundades ja antud efekt on suurem lühematel lainepikkustel. Suuremate osakeste valguse hajutamise protsess on keerulisem. Mida rohkem valgust hajutatakse tagasi veepinnalt, seda tugevam signaal jõuab ka satelliidisensorini.

Selle töö põhieesmärk oli uurida heljumi dünaamika ja optiliste omaduste varieeruvust optiliselt keerukates vetes, et paremini mõista nende mõju kaugseire signaalile ja veekeskkonnale.

Uurimiseesmärgid olid järgnevad:

– Uurida heljumi optiliste omaduste muutlikkust erinevates keskkonnaoludes Läänemere optiliselt keerukates rannikuvetes
– Iseloomustada heljumi osakeste tagasihajumise/hajumise suhet dünaamilistes ja optiliselt keerukates rannikuvetes, et täiustada kaugseire meetodeid

– Katsetada, kas optiliste veetüüpide põhine lähenemine võimaldab paremini hinnata heljumi dünaamikat, kui empiiriliste algoritmide kasutamine
– Uurida heljumi ruumilist jaotust dünaamilistes optiliselt keerukates rannikuvetes
– Uurida tormi mõju heljumi osakeste suurusjaotusele riimveelisel rannikualal
– Uurida traalimise järgset heljumi osakeste käitumist ja mõju keskkonnale reostunud rannikualal

Heljumi osakeste optiliste omaduste ja dünaamika ajalis-ruumiline varieeruvus Eesti rannikuvetes oli suur. See näitab, et osakeste koostis ja päritolu muutusid vastavalt oludele (nt. õitseng, torm).

Modelleerimise tulemused näitasid, et optiliselt keerukates vetes ei saa kasutada fikseeritud tagasihajumise/hajumise suhet. Oluline on koguda rohkem andmeid, teadmaks, millises vahemikus see suhe kuskil muutub, et seda kaugseire algoritmides vastavalt arvesse võtta.

Kuna Pärnu lahe optilised omadused on kiiresti varieeruvad, siis on keeruline korrektseks heljumi dünaamika hindamiseks kasutada vaid ühte empiirilist mudelit. Optiliste veetüüpide klassifikatsioonil põhinev meetod, mida rakendati Sentinel-3 piltide uurimiseks võimaldas hästi jälgida Pärnu lahe heljumi dünaamikat erinevates oludes (rahulik ilm, jõe mõju, tormid). Veelgi detailsem heljumi omaduste uurimine võimaldaks parendada heljumi kontsentratsiooni hindamise meetodeid.

Lisaks eelnevatele uuringutele, leidsime, et osakesed agregeerisid omavahel ka riimveelises Pärnu lahes (< 10 μm suurused osakesed liitusid > 30 μm suurusteks osakesteks).

Portmáni lahes uuriti detailsemalt heljumi mõju keskkonnale. Pärast traalimist olid setete ja setetes olevate raskemetallide kontsentratsioonid kõrged. Fe, Pb ja As liituvad kergesti väikeste algosakeste külge. Väikesed osakesed jäid veemassi hõljuma pikemalt kui suured osakesed, suurendades metalli/setete kontsentratsioonide suhet.

Traalimise järgsed settepilved laienesid suurele alale ja väikesed heljumi osakesed jäid veemassi hõljuma kauemaks kui kolm tundi. Seega aitas katse hinnata, kui kaugele ja kui kauaks põhjasetete üles keerutamise potentsiaalne ökotoksiline mõju keskkonnale avaldub.

Käesolevas töös uuriti detailselt mõningaid heljumi omadusi erinevates tingimustes. Saadud teadmisi saab kasutada, et uurida nende omaduste mõju kaugseire signaalile ja luua paremini töötavaid kaugseire algoritme. See töö võimaldas koguda andmeid ja teha lisavaatlusi tagasihajumise/hajumise suhte kohta, millega seoses on veel palju määramatusi (nt. spektraalne varieeruvus, sõltuvus osakeste suurusjaotustest, jm). Lisaks näitas Portmáni lahe eksperiment, et lähenemist, mille käigus uuriti raskemetallidega seotud heljumi keskkonnamõju veekogus, saab kasutada süvamere kaevandustegevuste keskkonnamõju hindamiseks.

ACKNOWLEDGMENTS

This study was supported by the Republic of Estonia, the Ministry of Education, the Estonian Research Council (grants PUTJD719, PRG302, PSG10), and the European Union's Horizon 2020 Research and Innovation Program (grant number 730066). The Portman Bay experiment was developed as part of the project MIDAS (Managing impacts of deep-sea resource exploitation) funded by the European Commission's 7th Framework Programme under the theme "Sustainable management of Europe's deep sea and sub-seafloor resources" (Grant Agreement 603418).

I am very grateful to my supervisors, Dr. Martin Ligi, Dr. Tiit Kutser, and Dr. François Bourrin, who always gave me advice and support. Writing scientific texts in English is a big challenge for me. Therefore, I am grateful that my supervisors took the time to review and correct my manuscripts and presentations and helped me to improve my writing. François kindly provided the LISST-100X instrument and training that allowed us to get valuable data for the innovative part of this study. Tiit added his invaluable knowledge of water's optical properties and provided the necessary instruments for the fieldwork. Martin was a valuable support in organising fieldwork, developing research ideas, and preparing for conference participation.

I thank all my colleagues at the Tartu Observatory, especially the Remote Sensing of Waters working group (Kristi, Krista, Kersti, Ave, Ian, Anu, Reiko). They made the working environment so pleasant and motivating and helped me with various issues, organising fieldwork and data collection.

I am grateful to my friends and family, who supported and encouraged me during these studies.

PUBLICATIONS

CURRICULUM VITAE

Name: Mirjam Uusõue
Date of birth: 24.04.1990
Nationality: Estonian
E-mail: mirjam.uusoue@ut.ee

Education:

Since 2017	University of Tartu, Faculty of Science and Technology, Estonian Marine Institute, PhD student in environmental technology
2013–2015	University of Perpignan (France), Faculty of Science and Technology, MSc in marine geosciences and aquatic environments
2010–2013	University of Perpignan (France), Faculty of Science and Technology, BSc in Earth and environmental sciences
2007–2010	Lycée Pablo Picasso, Perpignan, France

Professional employment:

Since 2022	Tartu Observatory, University of Tartu, Department of Remote Sensing, Engineer
2017–2022	Tartu Observatory, University of Tartu, Department of Remote Sensing, Junior Research Fellow
2016–2017	Tartu Observatory, Department of Remote Sensing, Technician

Scientific and research activity
Optical properties of suspended particulate matter

Additional courses
Baltic Earth Summer School "Climate of the Baltic Sea Region", Askö, Sweden, 28.08.–04.09.2017
Advanced Training School on Remote Sensing, Võru, Estonia, 15.–20.09.2019

Publications
Uusõue, M., Ligi, M., Kutser, T., Bourrin, F., Uudeberg, K., Kangro, K., Paavel, B. (2022). Effects of different conditions on particle dynamics and properties in West-Estonian coastal areas. *Oceanologia*. https://doi.org/10.1016/j.oceano.2022.06.006

Bourrin, F., **Uusõue, M.,** Artigas, M.C., Sànchez-Vidal, A., Aubert, D., Menniti, C., Klar, J. (2021). Release of particles and metals into seawater following sediment resuspension of a coastal mine tailings disposal off Portm´an Bay, Southern Spain. *Environmental Science and Pollution Research* 28, 47973–47990, https://doi.org/10.1007/s11356-021-14006-1

Uudeberg, K., Aavaste, A., Kõks, K.-L., Ansper, A., **Uusõue, M.,** Kangro, K., Ansko, I., Ligi, M., Toming, K., Reinart, A. (2020). Optical water type guided approach to estimate optical water quality parameters. *Remote Sensing* 12, 931, https://doi.org/10.3390/rs12060931

Additional publications

Tallobre, C., Loncke, L., Droz, L., Marsset, T., Uusõue, M., Roest, W.R., Fanget, A.-S., Bassetti, M.-A., Giresse, P., Bayon, G. (2021). Echo-facies interpretation of Pleistocene to Holocene contourites on the Demerara plateau and abyssal plain. Interpretation, 9 (2), SB49–SB65, 10.1190/INT-2020-0159.1.

Jiang, D., Matsushita, B., Pahlevan, N., Gurlin, D., Lehmann, M.K., Fichot, C.G., Schalles, J., Loisel, H., Binding, C., Zhang, Y., Alikas, K., Kangro, K., Uusõue, M., Ondrusek, M., Greb, S., Moses, W.J., Lohrenz, S., O'Donnell, D. (2021). Remotely estimating total suspended solids concentration in clear to extremely turbid waters using a novel semi-analytical method. Remote Sensing of Environment, 258, 112386. 10.1016/j.rse.2021.112386.

Balasubramanian, S.V., Pahlevan, N., Smith, B., Binding, C., Schalles, J., Loisel, H., Gurlin, D., Greb, S., Alikas, K., Randla, M., Bunkei, M., Moses, W., Ha N., Lehmann, M.K., O'Donnell, D., Ondrusek, M., Han, T.-H., Fichot, C.G., Moore, T., Boss, E. (2020). Robust algorithm for estimating total suspended solids (TSS) in inland and nearshore coastal waters. Remote Sensing of Environment, 246, ARTN 111768. 10.1016/j.rse.2020.111768.

Randla, M., Uudeberg, K., Ligi, M., Bourrin, F. (2018). Heljumi omaduste ja dünaamika varieerumine Pärnu lahes. Peterson, Urmas; Lillemaa, Tiia (Toim.). Kaugseire Eestis 2018, 2018, 41–50.

ELULOOKIRJELDUS

Nimi: Mirjam Uusõue
Sünniaeg: 24.04.1990
Kodakondsus: Eestlane
E-post: mirjam.uusoue@ut.ee

Haridus

Alates 2017	Tartu Ülikool, Loodus- ja täppisteaduste valdkond, Eesti Mereinsituut, doktorantuur keskkonnatehnoloogias
2013–2015	Perpignan'I Ülikool (Prantsusmaa), Loodus- ja tehnoloogiateaduskond, magister (Meregeoloogia ja veekeskkonnad)
2010–2013	Perpignan'i Ülikool (Prantsusmaa), Loodus- ja tehnoloogiateaduskond, bakalaureus (Maa- ja keskkonnateadused)
2007–2010	Lycée Pablo Picasso, Perpignan, France (keskkool)

Teenistuskäik

Alates 2022	Tartu observatoorium, Tartu Ülikool, Kaugseire osakond, Insener
2017–2022	Tartu observatoorium, Tartu Ülikool, Kaugseire osakond, Nooremteadur
2016–2017	Tartu observatoorium, Kaugseire osakond, Tehnik

Peamised uurimissuunad
Heljumi optilised omadused

Täiendkursused
Baltic Earth Suvekool "Climate of the Baltic Sea Region", Askö, Rootsi, 28.08.–04.09.2017
Advanced Training School on Remote Sensing, Võru, Estonia, 15.–20.09.2019

Publikatsioonid
Uusõue, M., Ligi, M., Kutser, T., Bourrin, F., Uudeberg, K., Kangro, K., Paavel, B. (2022). Effects of different conditions on particle dynamics and properties in West-Estonian coastal areas. *Oceanologia*. https://doi.org/10.1016/j.oceano.2022.06.006

Bourrin, F., **Uusõue, M.,** Artigas, M.C., Sànchez-Vidal, A., Aubert, D., Menniti, C., Klar, J. (2021). Release of particles and metals into seawater following sediment resuspension of a coastal mine tailings disposal off Portm´an Bay, Southern Spain. *Environmental Science and Pollution Research* 28, 47973–47990, https://doi.org/10.1007/s11356-021-14006-1

Uudeberg, K., Aavaste, A., Kõks, K.-L., Ansper, A., **Uusõue, M.,** Kangro, K., Ansko, I., Ligi, M., Toming, K., Reinart, A. (2020). Optical water type guided approach to estimate optical water quality parameters. *Remote Sensing* 12, 931, https://doi.org/10.3390/rs12060931

Muud publikatsioonid

Tallobre, C., Loncke, L., Droz, L., Marsset, T., Uusõue, M., Roest, W.R., Fanget, A.-S., Bassetti, M.-A., Giresse, P., Bayon, G. (2021). Echo-facies interpretation of Pleistocene to Holocene contourites on the Demerara plateau and abyssal plain. Interpretation, 9 (2), SB49–SB65, 10.1190/INT-2020-0159.1.

Jiang, D., Matsushita, B., Pahlevan, N., Gurlin, D., Lehmann, M.K., Fichot, C.G., Schalles, J., Loisel, H., Binding, C., Zhang, Y., Alikas, K., Kangro, K., Uusõue, M., Ondrusek, M., Greb, S., Moses, W.J., Lohrenz, S., O'Donnell, D. (2021). Remotely estimating total suspended solids concentration in clear to extremely turbid waters using a novel semi-analytical method. Remote Sensing of Environment, 258, 112386. 10.1016/j.rse.2021.112386.

Balasubramanian, S.V., Pahlevan, N., Smith, B., Binding, C., Schalles, J., Loisel, H., Gurlin, D., Greb, S., Alikas, K., Randla, M., Bunkei, M., Moses, W., Ha N., Lehmann, M.K., O'Donnell, D., Ondrusek, M., Han, T. H., Fichot, C.G., Moore, T., Boss, E. (2020). Robust algorithm for estimating total suspended solids (TSS) in inland and nearshore coastal waters. Remote Sensing of Environment, 246, ARTN 111768. 10.1016/j.rse.2020.111768.

Randla, M., Uudeberg, K., Ligi, M., Bourrin, F. (2018). Heljumi omaduste ja dünaamika varieerumine Pärnu lahes. Peterson, Urmas; Lillemaa, Tiia (Toim.). Kaugseire Eestis 2018, 2018, 41–50.

DISSERTATIONES TECHNOLOGIAE CIRCUMIECTORUM UNIVERSITATIS TARTUENSIS

1. **Sille Teiter**. Emission rates of N_2O, N_2, CH_4 and CO_2 in riparian grey alder forests and subsurface flow constructed wetlands. Tartu, 2005, 134 p.
2. **Kaspar Nurk**. Relationships between microbial characteristics and environmental conditions in a horizontal subsurface flow constructed wetland for wastewater treatment. Tartu, 2005, 123 p.
3. **Märt Öövel**. Performance of wastewater treatment wetlands in Estonia. Tartu, 2006, 148 p.
   Sergei Yurchenko. Determination of some carcinogenic contaminants in food. Tartu, 2006, 143 p. Published in *Dissertation Chimicae Universitatis Tartuensis,* 51.
4. **Alar Noorvee**. The applicability of hybrid subsurface flow constructed wetland systems with re-circulation for wastewater treatment in cold climates. Tartu, 2007, 117 p.
   Ülle Jõgar. Conservation and restoration of semi-natural floodplain meadows and their rare plant species. Tartu, 2008, 99 p. Published in *Dissertation Biologicae Universitatis Tartuensis*, 139.
5. **Christina Vohla**. Phosphorus removal by various filter materials in subsurface flow constructed wetlands. Tartu, 2008, 103 p.
6. **Martin Maddison**. Dynamics of phytomass production and nutrient standing stock of cattail and its use for environment-friendly construction. Tartu, 2008, 87 p.
7. **Marika Truu**. Impact of land use on microbial communities in Estonian soils. Tartu, 2008, 126 p.
8. **Elar Põldvere**. Removal of organic material, nitrogen and phosphorus from wastewater in hybrid subsurface flow constructed wetlands. Tartu, 2009, 107 p.
9. **Margit Kõiv**. Treatment of landfill leachate and municipal wastewater in subsurface flow filters using mineralized peat and hydrated oil shale ash. Tartu, 2010, 147 p.
10. **Jaanis Juhanson**. Impact of phytoremediation and bioaugmentation on the microbial community in oil shale chemical industry solid waste. Tartu, 2010, 95 p.
    Aare Selberg. Evaluation of environmental quality in Northern Estonia by the analysis of leachate. Tartu, 2010, 117 p. Published in *Dissertation Chimicae Universitatis Tartuensis,* 99.
11. **Riho Mõtlep**. Composition and diagenesis of oil shale industrial solid wastes. Tartu, 2010, 127 p.
12. **Igor Zaytsev**. Bioaugmentation in LWA-filled horizontal subsurface flow filters for wastewater treatment: Impact of flow regime, temperature and donor system Tartu, 2010, 97 p.

13. **Siiri Velling**. Microbial BOD biosensor for wastewater analysis. Tartu, 2011, 79 p.
14. **Riina Lepik**. Biodegradability of phenolic compoundsas single and mixed substrates by activated sludge. Tartu, 2011, 153 p.
15. **Liis Marmor**. Ecology and bioindicative value of epiphytic lichens in relation to air pollution and forest continuity. Tartu, 2011, 98 p.
16. **Martin Liira**. Active filtration of phosphorus in Ca-rich hydrated oil shale ash: precipitation mechanisms and recovery. Tartu, 2012, 84 p.
17. **Kristjan Karabelnik**. Advanced design and management of hybrid constructed wetlands: environmental and water purification effects. Tartu, 2012, 128 p.
18. **Hiie Nõlvak**. Influence of qPCR workflow on target gene enumeration from environmental samples in the case of bioremediation potential estimation. Tartu, 2012, 136 p.
19. **Merlin Raud**. Study of semi-specific BOD biosensors for biosensor-array. Tartu, 2013, 103 p.
20. **Ivar Zekker**. Enrichment of anaerobic ammonium oxidizing bacteria for nitrogen removal from digester effluent and anammox process acceleration by intermediate compounds. Tartu, 2013, 142 p.
21. **Annika Uibopuu**. Communities of arbuscular mycorrhizal fungi in spruce forest ecosystem and their effect on performance of forest understorey plant species. Tartu, 2013, 104 p.
22. **Jekaterina Jefimova**. Leaching of polycyclic aromatic hydrocarbons (PAHs) and heavy metals from the oil shale processing wastes and from waste-based products. Tartu, 2015, 184 p.
23. **Teele Ligi**. Bacterial community structure and its genetic potential for nitrogen removal in the soils and sediments of a created riverine wetland complex. Tartu, 2015, 127 p.
24. **Kuno Kasak**. Greenhouse gas emissions and water treatment efficiency in subsurface flow filters using various substrates. Tartu, 2016, 128 p.
25. **Martin Ligi**. Application of close range remote sensing for monitoring aquatic environment. Tartu, 2017, 146 p.
26. **Mikk Espenberg**. Impact of management on peatland microbiome and greenhouse gas emissions. Tartu, 2017, 152 p.
27. **Jens-Konrad Preem**. Forest soil bacterial community analysis using high-throughput amplicon sequencing. Tartu, 2017, 108 p.
28. **Taavi Vaasma**. Enrichment, atmospheric dispersion and deposition of naturally occurring radionuclides from oil shale-fired power plants. Tartu, 2017, 175 p.
29. **Kristjan Oopkaup**. Microbial community and its relationship with pollutant removal in treatment wetlands. Tartu, 2018, 154 p.
30. **Ergo Rikmann**. Autotrophic nitrogen removal and relevant equilibrial processes. Tartu, 2019, 179 p.
31. **Kati Klein**. Studies and treatment of inhibitory and recalcitrant wastewater. Tartu, 2021, 168 p.

32. **Thomas Schindler**. Tree stem CH_4 and N_2O fluxes in various forest ecosystems. Tartu, 2021, 182 p.
33. **Peeter Paaver**. Development of alternative binders based on oil shale fly ash. Tartu, 2021, 130 p.
34. **Kertu Tiirik**. Antibiotic resistance in connected engineered and natural aquatic environments. Tartu, 2021, 124 p.
35. **Keit Kill**. Nutrient fluxes regulation in an in-stream constructed wetland treating polluted agricultural runoff. Tartu, 2022, 144 p.
36. **Rauno Lust**. Bioelectrochemical systems for enhanced removal of nitrate from water with a low electron donor concentration. Tartu, 2022, 145 p.
37. **Mihhail Fetissov**. Spatial decision support systems for ecosystem-based marine management. Tartu, 2022, 172 p.
38. **Mohit Masta**. Isotopologue and microbiome studies for N_2O source attribution in peat soils. Tartu, 2022, 113 p.